

AD-A098 543

NORTHROP CORP HAWTHORNE CALIF AIRCRAFT DIV

F/S 14/2

IMPROVED LOW FREQUENCY EDDY CURRENT INSPECTION FOR CRACKS UNDER--ETC(U)

OCT 80 D T MIH

F33615-79-C-5054

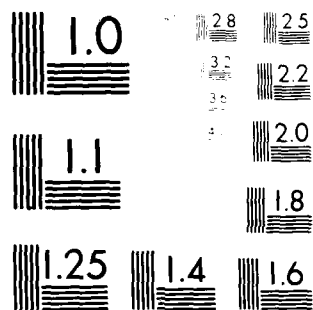
UNCLASSIFIED NOR-80-142

AFWAL-TR-80-4150

NL

1 OF 1
AD-A
11/14/81

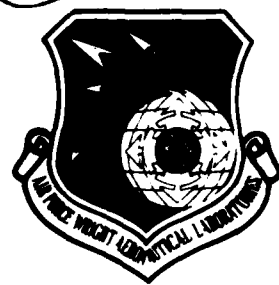
END
6-81



Microcopy Resolution Test Chart
ANSI Standard Z39.48-1968

AD A098543

18 AFWAL TR-80-4150



6 IMPROVED LOW FREQUENCY EDDY CURRENT
INSPECTION FOR CRACKS UNDER
INSTALLED FASTENERS.

10 D. T./MIH

NORTHROP CORPORATION
AIRCRAFT DIVISION
3901 WEST BROADWAY
HAWTHORNE, CALIFORNIA 90250

11 OCT 1980

12 90

14 NOR-80-142

7 TECHNICAL REPORT AFWAL-TR-80-4150
Final Report ~~1980~~ Jul 1979 - Oct 1980

DTIC
ELECTE
S MAY 6 1981

15 F33615-79-C-5054

16 2418

17 05 A

Approved for public release; distribution unlimited.

DTIC FILE COPY

MATERIALS LABORATORY (AFWAL/MLSA)
AIR FORCE WRIGHT AERONAUTICAL LABORATORIES
AIR FORCE SYSTEMS COMMAND
WRIGHT-PATTERSON AIR FORCE BASE, OHIO 45433


405228
81 5 06 130 m.t.

NOTICE

When Government drawings, specifications, or other data are used for any purpose other than in connection with a definitely related Government procurement operation, the United States Government thereby incurs no responsibility nor any obligation whatsoever; and the fact that the government may have formulated, furnished, or in any way supplied the said drawings, specifications, or other data, is not to be regarded by implication or otherwise as in any manner licensing the holder or any other person or corporation, or conveying any rights or permission to manufacture use, or sell any patented invention that may in any way be related thereto.

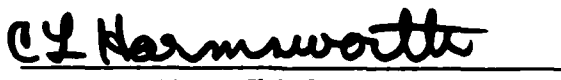
This report has been reviewed by the Office of Public Affairs (ASD/PA) and is releasable to the National Technical Information Service (NTIS). At NTIS, it will be available to the general public, including foreign nations.

This technical report has been reviewed and is approved for publication.


Project Engineer
Corrosion Control & Failure Analysis
Materials Integrity Branch


BENNIE COHEN, Technical Manager for
Corrosion Control & Failure Analysis
Materials Integrity Branch

FOR THE COMMANDER


C L HARMSWORTH, Chief
Materials Integrity Branch
Systems Support Division
Air Force Wright Aeronautical Laboratory

"If your address has changed, if you wish to be removed from our mailing list, or if the addressee is no longer employed by your organization please notify AFWAL/MLSA, W-PAFB, OH 45433 to help us maintain a current mailing list".

Copies of this report should not be returned unless return is required by security considerations, contractual obligations, or notice on a specific document.

REPORT DOCUMENTATION PAGE		READ INSTRUCTIONS BEFORE COMPLETING FORM	
1. REPORT NUMBER AFWAL-TR-80-4150	2. GOVT ACCESSION NO. AD-A098573	3. RECIPIENT'S CATALOG NUMBER	
4. TITLE (and Subtitle) Improved Low Frequency Eddy Current Inspection for Cracks Under Installed Fasteners		5. TYPE OF REPORT & PERIOD COVERED Final Report July 1979 - October 1980	
7. AUTHOR(s) D.T. Mih		6. PERFORMING ORG. REPORT NUMBER NOR 80-142	
9. PERFORMING ORGANIZATION NAME AND ADDRESS Northrop Corporation 3901 W. Broadway Hawthorne, CA 90250		8. CONTRACT OR GRANT NUMBER(s) F33615-79-C-5054	
11. CONTROLLING OFFICE NAME AND ADDRESS Materials Laboratory (AFWAL/MLSA) AF Wright Aeronautical Laboratories, AFSC Wright-Patterson AFB, OH 45433		10. PROGRAM ELEMENT, PROJECT, TASK AREA & WORK UNIT NUMBERS Project No. 2418-05	
14. MONITORING AGENCY NAME & ADDRESS (if different from Controlling Office)		12. REPORT DATE October 1980	
		13. NUMBER OF PAGES 98	
		15. SECURITY CLASS. (of this report) Unclassified	
		15a. DECLASSIFICATION/DOWNGRADING SCHEDULE	
16. DISTRIBUTION STATEMENT (of this Report) Approved for public release; distribution unlimited.			
17. DISTRIBUTION STATEMENT (of the abstract entered in Block 20, if different from Report)			
18. SUPPLEMENTARY NOTES			
19. KEY WORDS (Continue on reverse side if necessary and identify by block number) Eddy current Low frequency Eddy Current (LFEC) Bolt hole Second layer crack Coil Multisegment probe			
20. ABSTRACT (Continue on reverse side if necessary and identify by block number) The purpose of this program was to establish the feasibility of using low frequency eddy current (LFEC) techniques to inspect the second layer of a built up aluminum structure for hole cracking, with the titanium fasteners installed. This program pursued two parallel approaches for low frequency eddy current inspection. One approach was with centered field excitation in the fastener hole. The second approach was with off-center field excitation in the fastener hole. The program consisted of two tasks. The first task			

20. ABSTRACT (Continued)

was to optimize the probes for both approaches, and involved analysis, design, optimization of probes, and testing of various unique driver/sensor combinations. The second task was to develop inspection techniques with the optimized probes on notched specimens containing flush-head titanium fasteners with appropriate signal processing and display.

It has been shown that it is feasible and practical to use LFEC multisegment or circular array probe to detect 0.1 inch radial depth notch underneath 0.25 inch thick aluminum alloy skin, with titanium fasteners in place.

PREFACE

This report was prepared by the Northrop Corporation, Aircraft Division, Hawthorne, California, under Contract No. F33615-79-C-5054, Project No. 2418-05. The contract was administered under the direction of Materials Laboratory, Wright-Patterson Air Force Base, Ohio. Mr. Grover Hardy was the Project Engineer.

The program was conducted at Northrop under the supervision of W.R. Sturrock, Program Manager, and D.T. Mih, Principal Investigator. The following people made contributions during this reporting period.

Design and Analysis (Consultant)	K.M. Lakin
Circuit Design	K.K. Tam
Probe Assembly and Specimen Fabrication	L. Heller
Probe Assembly	P. Ashby
Ferrite Core Fabrication (subcontract)	R. Ruitz, Ceramic Form, Inc.

Accession For
FBI'S CHAIR
100-1043
100-1043
100-1043

A

TABLE OF CONTENTS

SECTION	PAGE
1 INTRODUCTION	1
2 PROGRAM OBJECTIVE AND SCOPE	5
3 THEORETICAL CONSIDERATION AND DESIGN	7
3.1 Introduction	7
3.2 Theory	9
3.3 Implementation	13
4 EXPERIMENTAL	17
4.1 Probe Fabrication	17
4.2 Sample Configuration	24
4.3 Flaw Detection Technique	28
5 EXPERIMENTAL RESULTS	37
6 DISCUSSION OF RESULTS	55
7 CONCLUSIONS	57
8 RECOMMENDATIONS FOR FUTURE WORK	59
APPENDIX A PHOTOGRAPHS OF GFM	61
APPENDIX B GFM NOTCH DIMENSIONS	73

LIST OF ILLUSTRATIONS

FIGURE		PAGE
1	C-5A Wing-Splice Configuration	2
2	Top View of Eddy Current Around a Bolt Hole with Cylindrically Symmetric Excitation	7
3	Equivalent Circuit of a Simple Search Coil	8
4	Field Volume Used to Determine the Impedance of a Simple Coil Coupled to a Metal	9
5	Simple Cup-Core Coil Coupled to a Bolt Hole Having Fastener in Place.	10
6	Top Schematic View of Cup Core Over a Bolt Hole.	10
7	Side View of a Segmented Core.	11
8	Equivalent Circuit of a Multisegment Coil.	12
9	Three-Phase Coil	15
10	Two-Phase (Quad-Cup) Coil.	16
11	Multisegment Core Dimensions	18
12	A Multisegment Array Probe	19
13	Field Profile at Probe Surface	20
14	Field Profile 0.25 Inch From Probe Surface	20
15	Field Profile Away From Probe Surface.	21
16	Field Profile Away From Outer Segment.	21
17	Three-Phase Core	22
18	Potted Three-Phase Probe	23
19	Quad Cup Core.	24
20	Quad Cup Probe	25
21	Simulated C-5A Specimen (Type I)	26
22	Simulated C-5A Specimen (Type II).	26
23	Simulated C-5A Specimen (Type III)	27
24	Computerized Eddy Current Scanning System.	29
25	Probe Segments Scanning Scheme	30
26	GPB Interface Wiring Diagram.	31
27	Signal Expander/Level Shifter.	32

LIST OF ILLUSTRATIONS (Continued)

FIGURE		PAGE
28	Commercial Instrument Interface Diagram.	32
29	Centering Block Diagram.	33
30	Electronic Centering Schematics.	33
31	Laboratory Crack Detection Set-Up.	35
32	Hand-Held Inspection of GFM.	35
33	Detection Plot of Specimen 1	39
34	Linear Plot of Specimen 2.	39
35	Polar Plot of Specimen 2	40
36	Linear Plot of Specimen 3.	40
37	Polar Plot of Specimen 3	41
38	Linear Plot of Specimen 3.	41
39	Polar Plot of Specimen 3	42
40	Detection Plot of Specimen 4	42
41	Detection Plot of Specimen 5	43
42	Detection Plot of Specimen 5 at 300 Hz	43
43	Detection Plot of Specimen 5 at 500 Hz	44
44	Detection Plot of Specimen 5 at 600 Hz	44
45	Detection Plot of Specimen 5 at 700 Hz	45
46	Detection Plot of Specimen 6	45
47	Detection Plot of Specimen 7	46
48	Detection Plot of Specimen 7 with One Segment Offset	46
49	Detection Plot of Specimen 8 with One Segment Offset	47
50	Detection Plot of Specimen 9	47
51	Detection Plot of Specimen 10.	48
52	Detection Plot of Specimen 10 with One Segment Offset.	48
53	Detection Plot of Specimen 11.	49
54	Relative Segment Voltages for Type I Specimens	49
55	Detection Plot of GFM "Specimen A," Hole 2	50
56	Detection Plot of GFM "Specimen A," Hole 11.	50
57	Detection Plot of GFM "Specimen E," Hole 8	51
58	Detection Plot of GFM "Specimen E," Hole 10.	51
59	Detection Plot of GFM "Specimen I," Hole 10.	52
60	Detection Plot of GFM "Specimen I," Hole 6	52

LIST OF ILLUSTRATIONS (Concluded)

FIGURE		PAGE
61	Detection Plot of GFM "Specimen I," Hole 15.	53
62	Detection Plot of an Outer Layer Flaw.	53
A-1	Photographs of GFM "Specimen A".	63
A-2	Photographs of GFM "Specimen B".	64
A-3	Photographs of GFM "Specimen C".	65
A-4	Photographs of GFM "Specimen D".	66
A-5	Photographs of GFM "Specimen E".	67
A-6	Photographs of GFM "Specimen F".	68
A-7	Photographs of GFM "Specimen G".	69
A-8	Photographs of GFM "Specimen H".	70
A-9	Photographs of GFM "Specimen I".	71
A-10	Photographs of GFM "Specimen J".	72

LIST OF TABLES

TABLE		PAGE
1	Simulated C-5A Specimen List	27
B-1	GFM "Specimen A" Notch Dimensions.	75
B-2	GFM "Specimen B" Notch Dimensions.	76
B-3	GFM "Specimen C" Notch Dimensions.	77
B-4	GFM "Specimen D" Notch Dimensions.	78
B-5	GFM "Specimen E" Notch Dimensions.	79
B-6	GFM "Specimen F" Notch Dimensions.	80
B-7	GFM "Specimen G" Notch Dimensions.	81
B-8	GFM "Specimen H" Notch Dimensions.	82
B-9	GFM "Specimen I" Notch Dimensions.	83
B-10	GFM "Specimen J" Notch Dimensions.	84

SUMMARY

Present Low Frequency Eddy Current (LFEC) equipment is available with either general purpose probes or probes designed for the detection of large cracks emanating from fastener holes in second or interior layers. These existing probes interrogate the entire fastener hole during inspection and consequently are insensitive to the presence of small cracks.

This program demonstrated the feasibility of a LFEC technique where the fastener hole is scanned electromagnetically. Three probe designs were evaluated and the design consisting of a central driver coil surrounded by a circumferential series of receiver coils was able to detect a 0.1" radial depth crack underneath an outer layer of 0.25" thick aluminum with a titanium fastener in place. The probe, interfaced with an existing LFEC equipment and appropriate signal processing network, produced a circular display of the fastener hole with an inward radial excursion indicating the presence of a crack.

SECTION 1

INTRODUCTION

Span-wise splice joints between structural wing skins on cargo aircraft represent a structural configuration where fatigue damage can occur at the fastener hole in either skin (layer), Figure 1. Presently, two choices exist for the inspection of fastener holes in such structure. Either the fastener can be removed and the hole inspected with conventional eddy current techniques or shear wave ultrasonic methods can be utilized with the fastener intact. Neither choice is entirely satisfactory.

Eddy current fastener hole scanning can detect small flaws reliably but the fastener removal/re-installation is costly and a potential source of structural damage. Ultrasonic shear wave inspection is an effective method of inspecting the faying surface region of the outer skin (layer) but it is considerably less effective in the region of a fastener hole countersink. When a faying surface sealant is present, the ultrasonic shear wave technique has the potential of penetrating into the inner layer, but the reduction to practice of this inner layer inspection has not occurred. When this technique is developed, the faying surface side of the inner layer would not be as effectively inspected as the opposite side, and many structures exist that do not use sealants in a multi-layer configuration. Obviously, then, the requirement exists for an inspection technique that would complement the ultrasonic shear wave technique as well as not be dependent on the presence of sealant for inner layer inspections.

LFEC techniques offer the potential of fulfilling this need. They can complement the ultrasonic shear wave techniques by being more effective on the side of the layer nearest the outer or inspection surface. Also, they are not dependent upon sealant for inner layer inspection. Present LFEC techniques, however, lack the required sensitivity. Under ideal conditions, cracks of 0.2" radial depth can be detected under 0.25" of aluminum with a titanium fastener in place and this degrades to about 0.5" radial depth on real aircraft structure. In

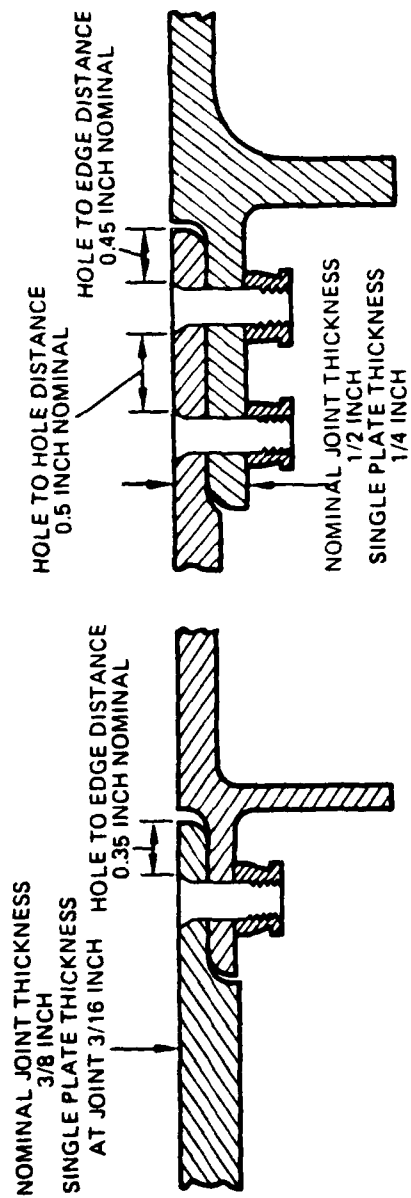


Figure 1. C-5 Wing-Splice Configuration

order to improve this capability to a 0.1" radial depth flaw under a 0.25" aluminum layer in real structure, the need remains as to develop a new, practical LFEC device to detect small fatigue cracks in the second layer of aluminum structure.

SECTION 2

PROGRAM OBJECTIVE AND SCOPE

The program objective is to develop a low-frequency eddy current technique to inspect inner layers of aluminum structure for cracking in holes with the fastener installed. The detection goals are 0.1-inch radial depth through-the-thickness crack in the inner layer, under a 0.25-inch thick outer layer with the titanium fastener installed.

The program conducted to accomplish this objective consisted of two major tasks:

Task I - Probe/Sensor Optimization

Task II - Inspection Technique Development.

The objective of Task I is to optimize new LFEC probe designs for the detection of second layer cracks. This was accomplished by analysis, design, fabrication, and testing of unique driver/sensor combinations.

The analysis involved theoretical models based on transformer and electromagnetic theory to optimize the electromagnetic conditions such as coupling, penetration, field shape, and power, to ensure that driver/sensor combinations are firmly based on sound physical principles.

The new probe designs involve both centered and noncentered approaches and involved novel driver and sensor configurations based on the preceding theoretical analysis.

The new coils were fabricated per the drawings with intermediate tests and measurements to ensure that design conditions such as inductance and field strength have been met prior to final assembly. Prototype probes were assembled and tested for proper configuration.

Results of testing of the various probe configurations on slotted specimens of various thicknesses and slot sizes, in addition to field strength and electrical parameter measurements, were compared to the design conditions. Where

unsatisfactory results were obtained, designs were modified in the direction indicated by analysis and modeling to improve the performance. New probe assemblies were fabricated and tested. By this means, the probe performance was optimized to detect second layer cracks.

The objective of Task II is to develop and display the detection of second layer cracks using the optimized probes and techniques suitable for rapid, reliable inspection of 0.1-inch cracks through an 0.25-inch thick outer layer. This task examined and tested electromagnetic and geometrical parameters affecting sensitivity of various probes and included novel, but low-cost, signal processing and display techniques to enhance signal to noise ratios and detection reliability.

The effectiveness of various probe configurations was demonstrated on the notched GFM specimens containing flush-head titanium fasteners. The demonstration showed the tolerance of the new technique to positioning errors, the insensitivity to lift-off, and the ease of calibration.

SECTION 3

THEORETICAL CONSIDERATION AND DESIGN

3.1 Introduction

The detection of cracks using eddy currents usually involves a kind of search coil which may be operated as a one terminal pair or two terminal pair device. The crack detection takes place when the otherwise normal eddy current distribution is upset by the localized presence of a flaw or crack, and the resultant change in magnetic flux is then sensed as a change in the inductance of the coil as shown in Figure 2.

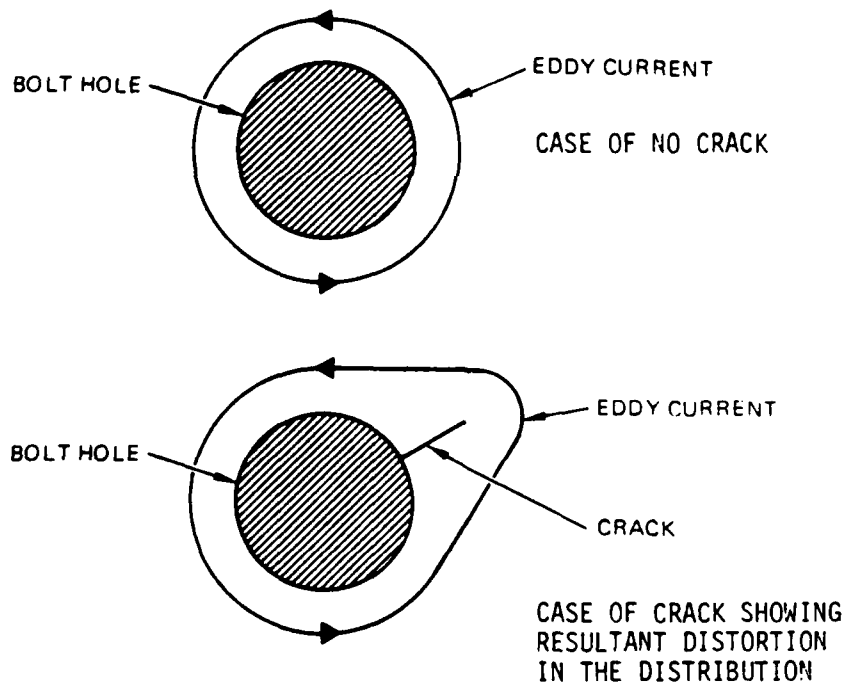


**Figure 2. Top View of Eddy Currents Around a Bolt Hole
with Cylindrically Symmetric Excitation**

The search coil also may be viewed as a transformer having a primary, main winding, and a secondary which is the eddy current circuit, Figure 3. The mutual inductance is determined by the degree of coupling to the eddy current region and the properties of the material such as the conductivity and permeability. If the coil is a one terminal pair, the input impedance of this circuit is determined by an integration of the fields within the whole volume, Figure 4. The boundaries must extend to the region of zero field intensity. The lumped element equivalents are given by:

$$L = \frac{\mu}{I^2} \int B^2 dv \quad \text{inductance} \quad (1)$$

$$C = \frac{\epsilon}{V^2} \int E^2 dv \quad \text{capacitance} \quad (2)$$

$$R = \frac{\sigma}{I^2} \int E^2 dv \quad \text{resistance.} \quad (3)$$

If the crack occupies a small fraction (0.0001) of the total field volume, the change in eddy current distribution will be small and the change in the coil impedance also small and difficult to measure.

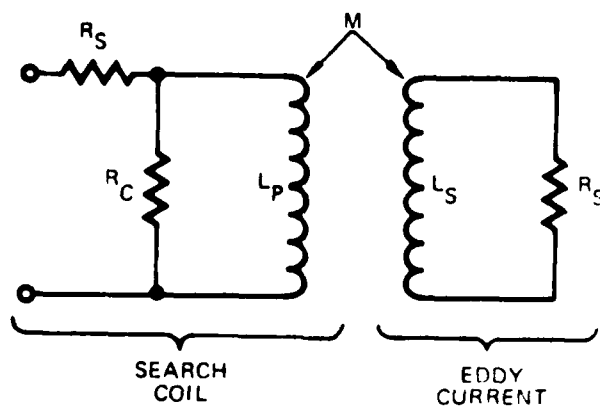


Figure 3. Equivalent Circuit of a Simple Search Coil

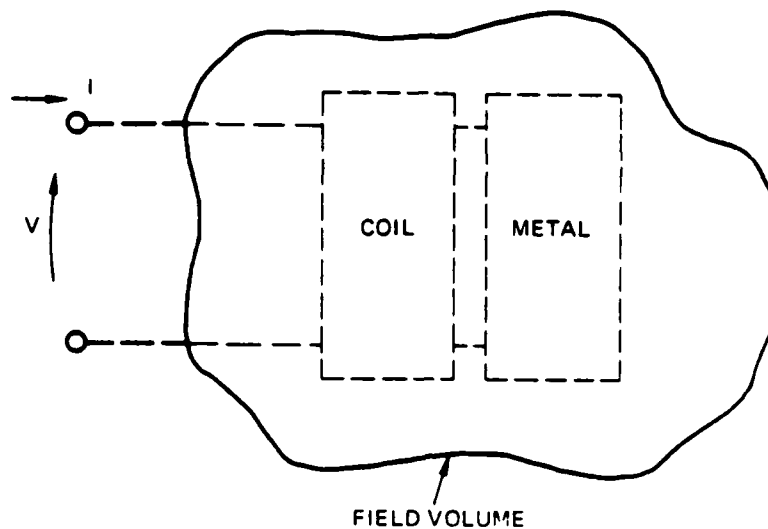
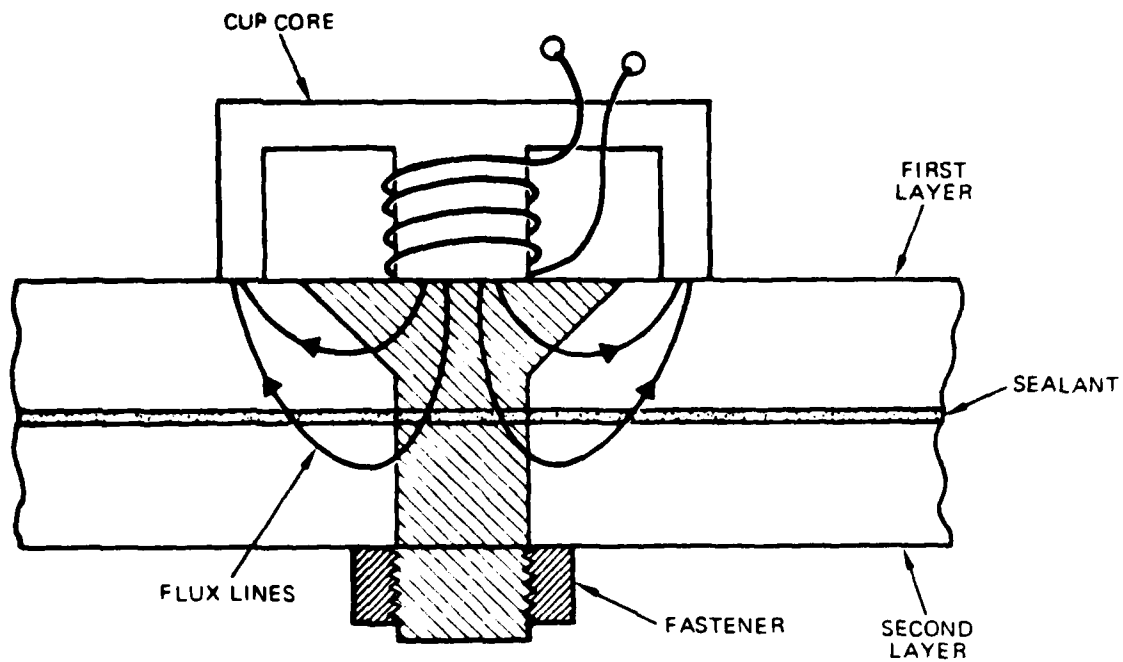


Figure 4. Field Volume Used to Determine the Impedance of a Simple Coil Coupled to a Metal

Since the simple terminal impedance is an integrated result, it is also influenced by non-flaw related effects. Such effects as coil lift off from surface, edge effects, and centering, in the case of bolt hole inspection, are much larger effects than the flaw itself. This is particularly true in the case of second surface cracks in bolt holes. When the cracked or flawed region is localized, it would be useful to have a probe that is sensitive to a local region yet also examines a larger area in a single probe placement. Three basic probe configurations were investigated in this program: one was the field scanning probe using multisegment arrays, the other was a rotating field probe using three-phase drive, and the third was a rotating field probe using two-phase drive.

3.2 Theory

In the case of a simple cup core probe, Figure 5, the flux lines close in a cylindrically symmetric manner in the absence of any perturbing influence. However, if a crack is located under one region of the core, Figure 6, the flux in that region will be disturbed locally. The net flux change through the center core, which is effectively an integral of the outer rim flux, may not change significantly.



**Figure 5. Simple Cup Core Coil Coupled to a Bolt Hole
Having Fastener in Place**

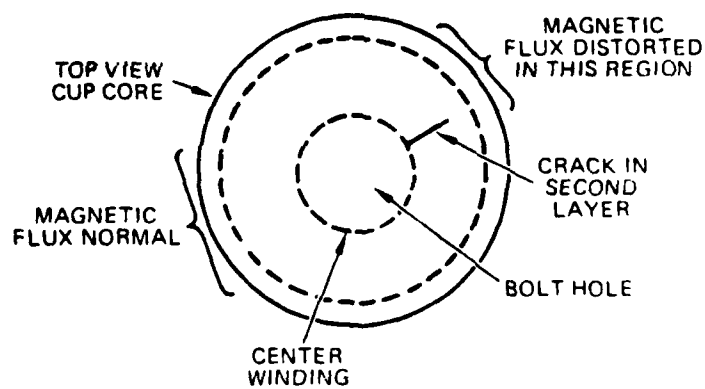


Figure 6. Top Schematic View of Cup Core Over a Bolt Hole

By placing other sense coils in the outer rim of the cup core, the localized flux disturbances may be more readily determined. The technique for doing this is using a standard cup core that has been drilled and slotted. The hole allows space for the segment windings and the slots provide access for winding the coils as well as keeping the external flux separated, Figure 7, until beyond the coils. From Figure 7, the segment coil voltages are given by:

$$V_n = \frac{d\psi_n}{dt} = j\omega\psi_n \quad (4)$$

$$V_{n+1} = \frac{d\psi_{n+1}}{dt} = j\omega\psi_{n+1} \quad (5)$$

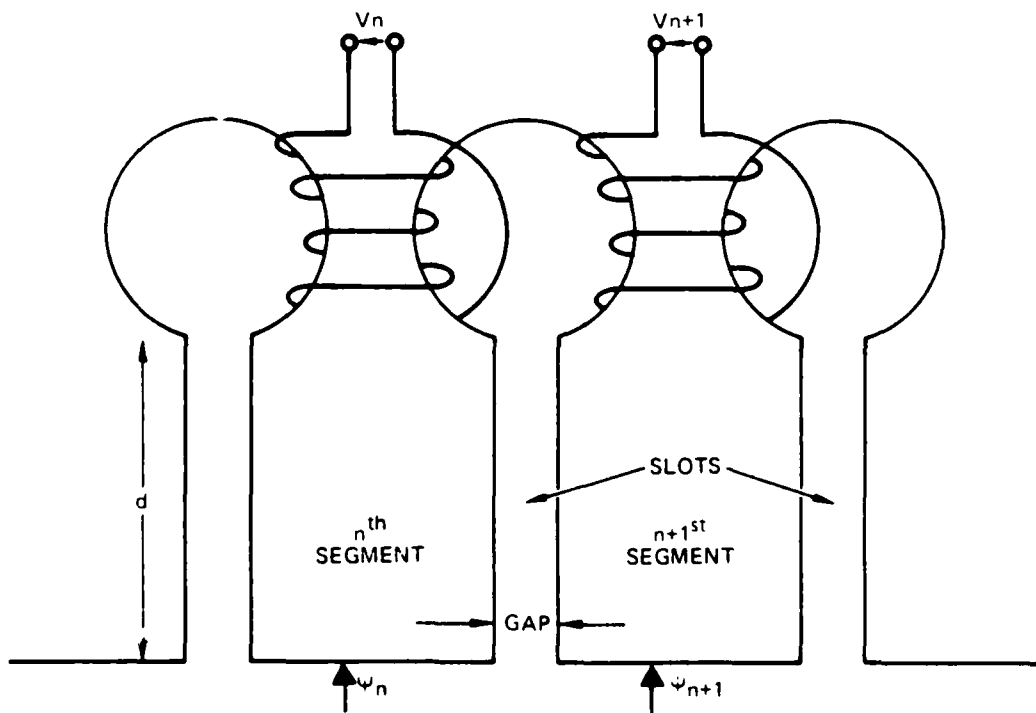


Figure 7. Side View of a Segmented Core

In this operating mode, the multisegment coil really becomes a secondary winding, Figure 8. The segment fluxes depend upon the reluctance of the path and determine the mutual inductances between the primary and various secondary windings. Thus in the presence of a crack, the segment voltages near the flawed region would be different than those away from the region. The difference voltage,

$$\Delta V_n = V_{n+1} - V_n \quad (6)$$

may be analyzed as a function of segment position or index, n , in order to determine the location and size of the flaw.

Since the segment voltages are also a function of other parameters such as lift off and slight differences in segment coil construction, the actual implementation will require some form of reference measurement.

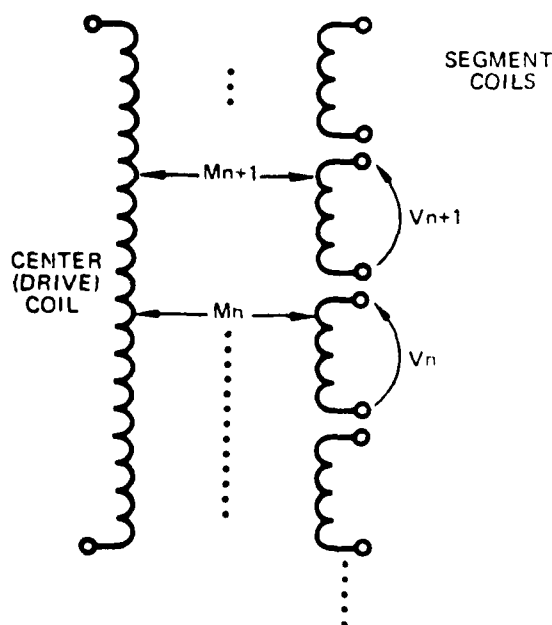


Figure 8. Equivalent Circuit of a Multi Segment Coil

3.3 Implementation

1. Field Scanning Probe - The most likely mode for the multisegment probe is to drive the center coil at the frequency of interest and measure the open circuit voltages at the segments. If these voltages are then recorded for a specimen without flaws and used as a reference for a flawed specimen, the difference may be used to determine the presence of a flaw. The difference voltage is given by:

$$V_{fn} = V_n^0 - V_n \quad (7)$$

where V_n^0 is the reference voltage measured without the flaw and V_n is the segment voltage with the flaw. By comparing the segment variations of V_{fn} the flaw location may be determined.

Four effects may significantly alter this simple picture; centering, geometrical distortion in hole, lift off, and edge effects. First, if the coil is not centered over the flawed specimen the same as for the reference specimen, the off centering itself will cause variations in V_{fn} between various segments. However, the center coil, when operated as a normal one terminal pair search coil at higher frequencies, can be used to center the coil over the bolt hole. Any slight off centering or geometrical distortions would result in gradual variations of the segment voltage as a function of position around the circumference. Similarly, lift off would also show variations of the segment voltages. However, a localized flaw, or any first layer crack, would produce more immediate effects in that segment nearest the flaw. Therefore, an examination of the rate of change of the voltage V_{fn} as a function of segment position could be used to separate the flaw effects from other effects.

In the case of second-surface crack detection in bolt holes with fasteners in place, the flaw-induced field changes are much smaller due to shielding by the first layer and the distance between crack and segments. In order to probe into the second layer region, lower frequencies must be employed. However, the lower frequency eddy currents also spread laterally and make the probe sensitive to the panel edges and adjacent bolt holes. The coil frequency is thus a critical parameter and must be chosen, if possible, to optimize the second layer crack detection. Again, it is important to distinguish the more rapid field variations caused by edge effects. But when the flaw signals are as small as those caused by coil placement errors, it may be necessary to do the

segment calibrations in place rather than on a separate reference specimen and then transferring to the specimen of interest. This procedure is required when the error voltage caused in inaccuracies in coil placement exceeds the voltage change due to the flaw itself. In-place calibration may be accomplished by operating the coil at a high frequency where the flaw and panel edge regions are cutoff due to skin effects. The variations between segment voltages may be accounted for as follows. In general the segment voltages may be written as:

$$V_n = V_n^0 + \Delta V_{no} + \Delta V_{nF} \quad (8)$$

where V_n^0 is the segment voltage with no flaw or alignment errors, ΔV_{no} is the error voltage due to alignment and coil fabrication variations, and ΔV_{nF} is the change due to the flaw and any other low frequency effect such as edges. At a high frequency where the flaw and edges are cutoff by skin effect,

$$V_n(fh) = V_n^0(fh) + \Delta V_{no}(fh) \quad (9)$$

At any other frequency, the voltage is just a constant multiple of $V_n(fh)$.

$$V_n(f) = K V_n(fh) \quad (10)$$

In other words, the ratios of segment voltages are assumed independent of frequency if the flaw or edge effects are not present. The dependence of K on frequency may be determined by measurements made on a carefully aligned reference sample. In the presence of a second-surface crack measured at a lower frequency,

$$V_n(f1) = K V_n(fh) + \Delta V_{nF} \quad (11)$$

or

$$\Delta V_{nF} = V_n(f1) - K V_n(fh) \quad (12)$$

The importance of the above procedure is that all of the right hand side of Equation 12 is measured within the same coil placement. Determining what part of the ΔV_{nF} is due to the flaw, as opposed to an edge effect, will require an analysis of the rate of voltage change with respect to segment position. Since the edge effects are more diffuse, the segment-to-segment variations should be smaller even though ΔV_{nF} might be largely caused by the edge effect. In this case the second surface crack should appear as a small segment-to-segment variation on top of the edge effect. The nature of the edge effect could be obtained by measurements made upon a reference sample as a function of frequency

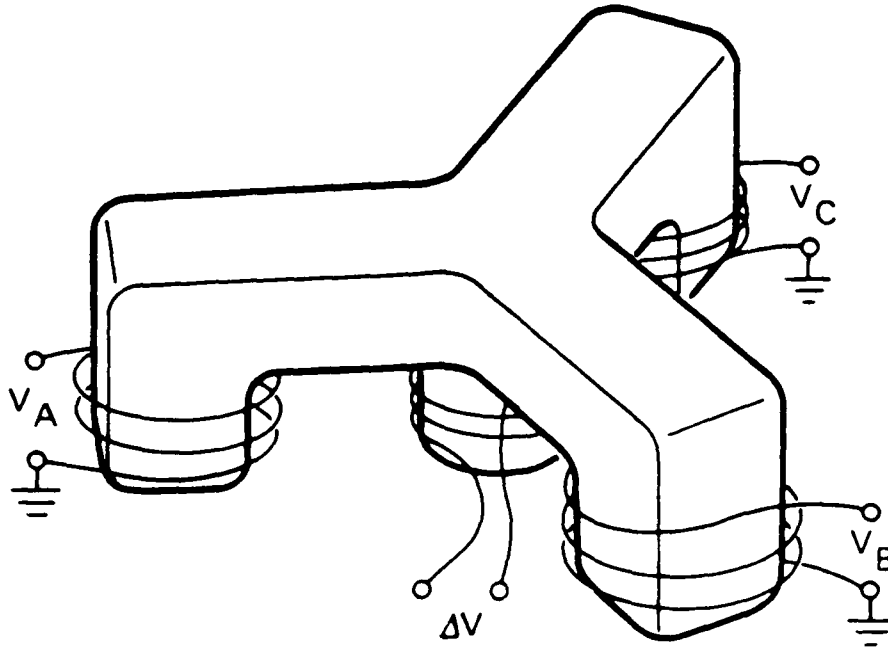


Figure 9. Three-Phase Coil

and compared to the case of a second surface crack.

2. Rotating Field Probe - The rotating field probes are similar to the multi-segment probe in that the region around the fastener is sampled without physical movement of the probe itself. Such a coil configuration is shown in Figure 9. The drive voltages are given by:

$$V_A = V_0 \cos \omega t$$

$$V_B = V_0 \cos (\omega t + 120) \quad (13)$$

$$V_C = V_0 \cos (\omega t + 240)$$

corresponding to a three-phase drive. This configuration is the same as the classic three-phase drive used in AC motors to obtain rotating magnetic field. The net error voltage, ΔV , resulting from the drive coils is zero due to the vector sum of the three flux contributions and because the center coil samples each flux. The error voltage is given by:

$$\Delta V = \frac{d}{dt} \int_A \vec{B}_A \cdot d\vec{s} + \int_B \vec{B}_B \cdot d\vec{s} + \int_C \vec{B}_C \cdot d\vec{s} \quad (14)$$

CENTER POLE OMITTED FOR CLARITY

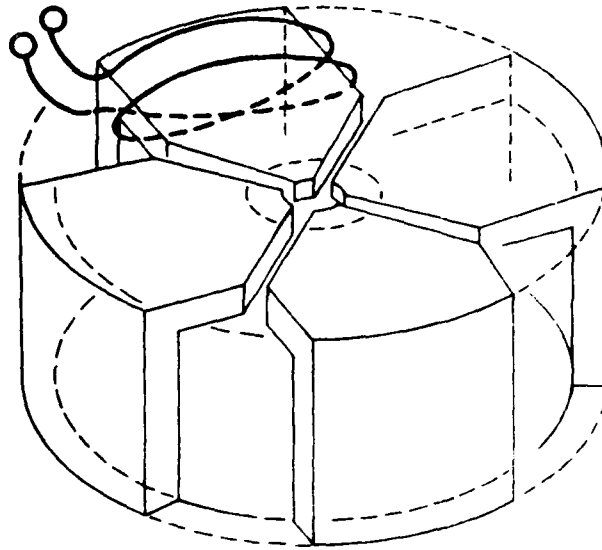


Figure 10. Two-Phase (Quad Cup) Coil

where the integrals are over the respective core areas corresponding to the field due to the three drive signals. A slight adjustment of the drive voltages can be used to adjust ΔV to zero to compensate for any fabrication asymmetries in the coils. If the flux induced by the eddy currents is also perfectly symmetric, ΔV is also zero. However, any asymmetry due to a crack will cause a finite ΔV .

However, both the three-phase and two-phase (quad cup) coils, Figure 10, integrate the flux over a much larger region than the multisegment coil because the coils are much larger. A 16 segment coil has over five times the angular resolution of the three-phase coil system.

SECTION 4

EXPERIMENTAL

4.1 Probe Fabrication

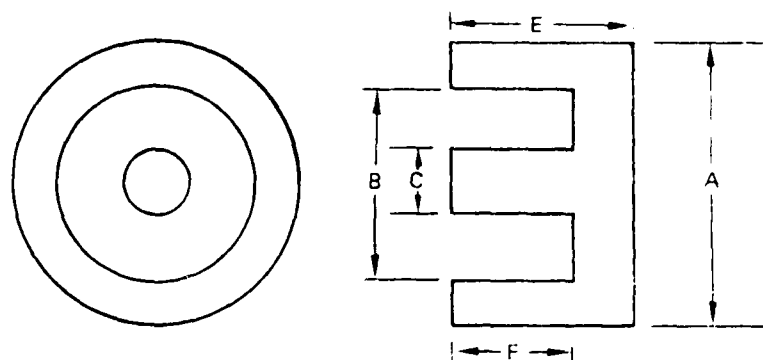
The unique designs that resulted from the analysis and design effort were used in coil fabrication and assembly. The probe construction sequence consisted of four basic steps:

- Core Fabrication
- Coil Winding
- Intermediate Test
- Final Probe Assembly

Multisegment Probe

Since there is no off-the-shelf part available with the proper dimensions, the cores have to be machined and fabricated from ferrite blanks. Machining of the ferrite material can be accomplished with diamond tools or ultrasonic abrasive tools. It was found that either of the above two methods for ferrite core fabrication gives good results. Figure 11 shows the core dimensions for various bolt hole diameters. The holes in the multisegment core were made by diamond drills and the slots were made by diamond wire saw. The holes allow space for the windings and the sawed gaps allow access to the holes for winding the segment coils as well as keeping the flux lines separated. The diameter of the holes varies from 35 mils to 65 mils depending on the size of the cores.

Due to the small size of the holes, 44 AWG size magnet wire with single polyurethane coating was used to wind coils. The polyurethane coating was chosen over a Formvar coating because polyurethane can be removed by chemical means. This is important because for fine magnet wires, insulation removal by chemical means gives results superior to other techniques such as heat or mechanical scraping. A plastic bobbin wound with 34 AWG magnet wire was



	BOLT HOLE DIAMETER		
	3/16 INCH	1/4 INCH	5/16 INCH
A	0.50	0.58	0.85
B	0.30	0.38	0.65
C	0.18	0.24	0.28
E	0.45	0.45	0.45
F	0.40	0.40	0.285

Figure 11. Multisegment Core Dimensions

slipped over the center pole of the core. The whole probe assembly was then mounted on a plexiglass support using RTV silicone adhesive.

A multifrequency digital impedance meter was used for intermediate test. Test parameters were coil inductance and resistance of each segment at frequency of interest. Any unacceptable segment was rewound. There were no guidelines for probe electrical parameters. A typical segment has an inductance value and resistance value of 1.13 mH and 14.7 ohms, respectively at 400 Hz. Maximum number of segment windings were limited by the hole diameters. Segment impedances or output voltages should be held within one percent of each other. But the impedance range of a center coil can be anywhere from 16 ohms to 75 ohms at the frequency of interest, without any major effect on the probe performance. A center coil has a typical inductance value of 8.5 mH and resistance value of 10.5 ohms at 400 Hz, with a resultant impedance of 24 ohms. If the test results were within design allowance, the probe was then ready for final assembly.

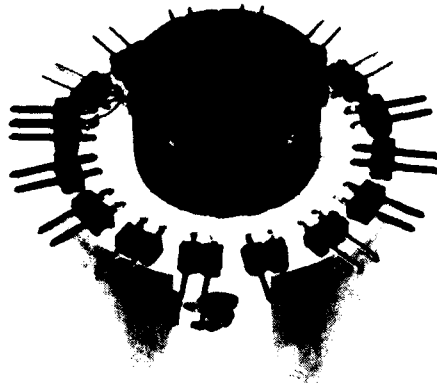


Figure 12. A Multisegment Array Probe

Two pin mating connectors were bonded around the edge of the plexiglass support with epoxy adhesive for electrical connections. Ends of wire pairs from center driver and side segments were soldered to the connectors. A typical assembled multisegment probe is shown in Figure 12. Field strength and field distribution were also measured. A gauss meter was used for this purpose. Typical field profiles are shown in Figure 13 for data taken at the probe surface and in Figure 14 for data taken 0.25-inch away and normal to the probe surface. On-axis field patterns are shown in Figure 15 for data taken at the center of the driving coil and in Figure 16 for data taken at the midpoint of the outer segment.

Three-Phase Probe

Ferrite pot cores were sectioned with a diamond saw into groups of three identical pieces. These pieces were then bonded together with epoxy adhesive to form a three-phase core as shown in Figure 17. A plastic bobbin wound with 38 AWG magnet wire was slipped over the center pole of the core. Three legs of the core were wound with 40 AWG magnet wire.

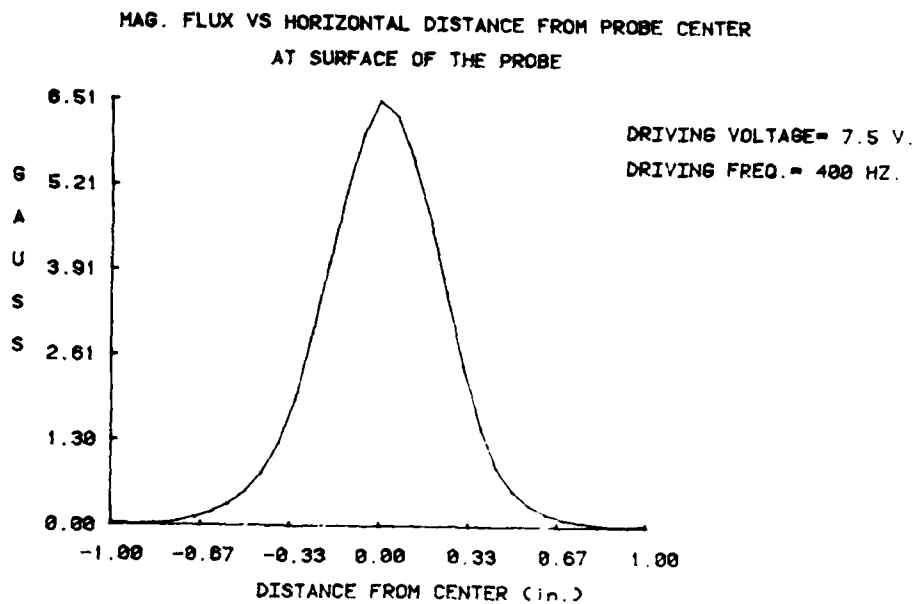


Figure 13. Field Profile Across Probe Surface

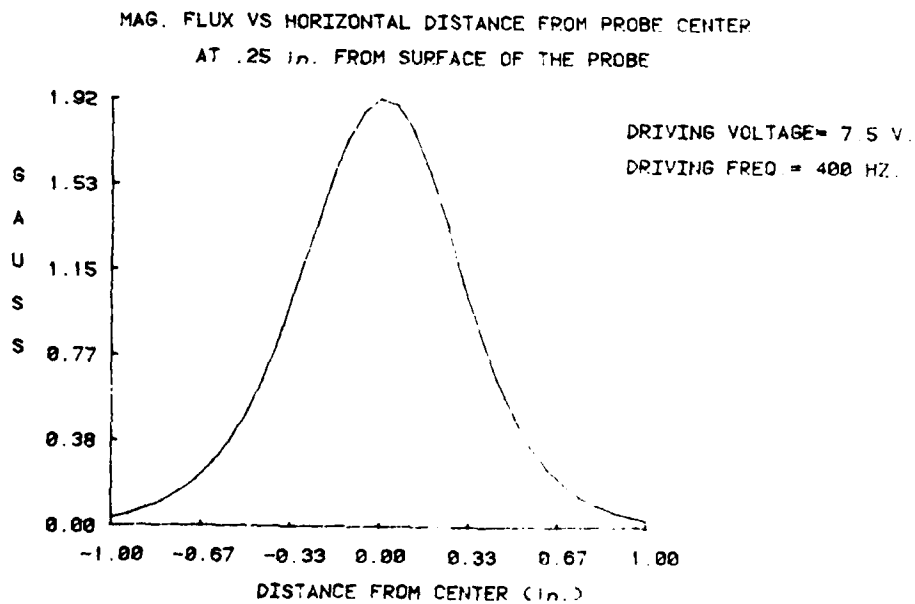


Figure 14. Field Profile 0.25 Inch From Probe Surface

MAG. FLUX VS NORMAL DISTANCE FROM PROBE CENTER

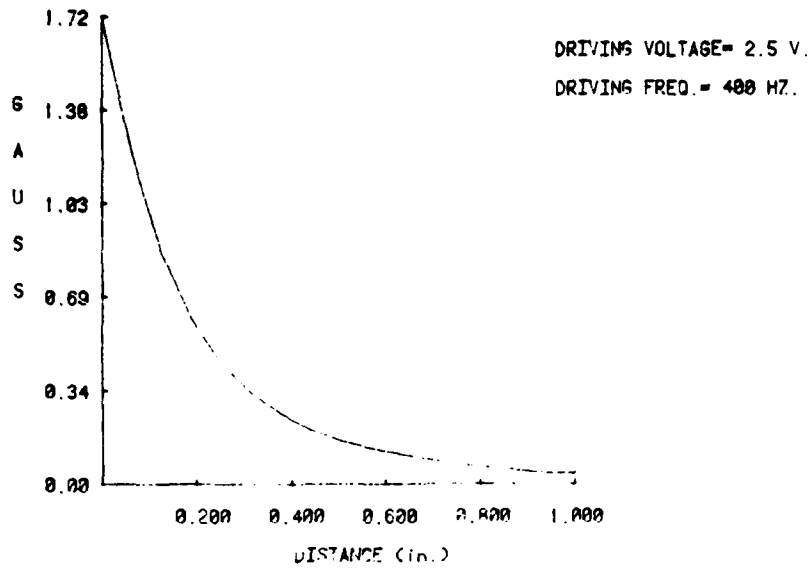


Figure 15. Field Profile Away From Probe Surface

MAG. FLUX VS NORMAL DISTANCE FROM AN OUTER SEGMENT

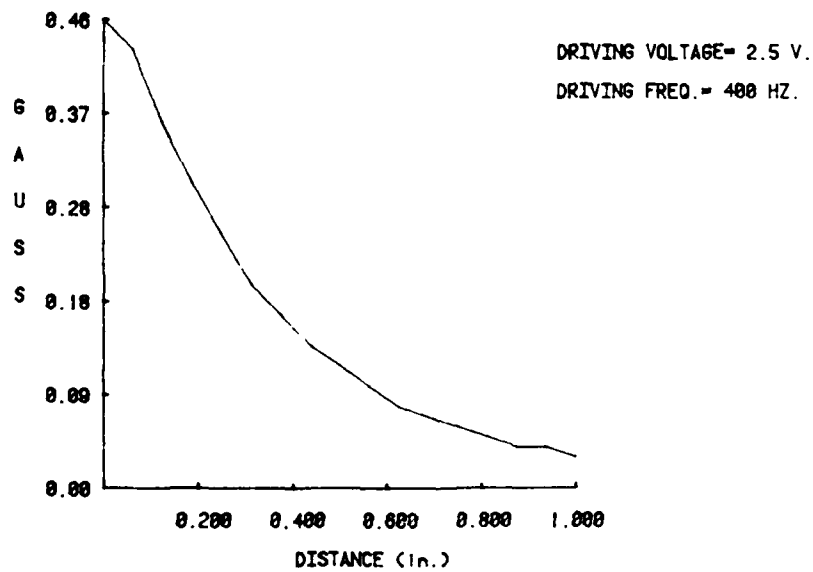


Figure 16. Field Profile Away From Outer Surface

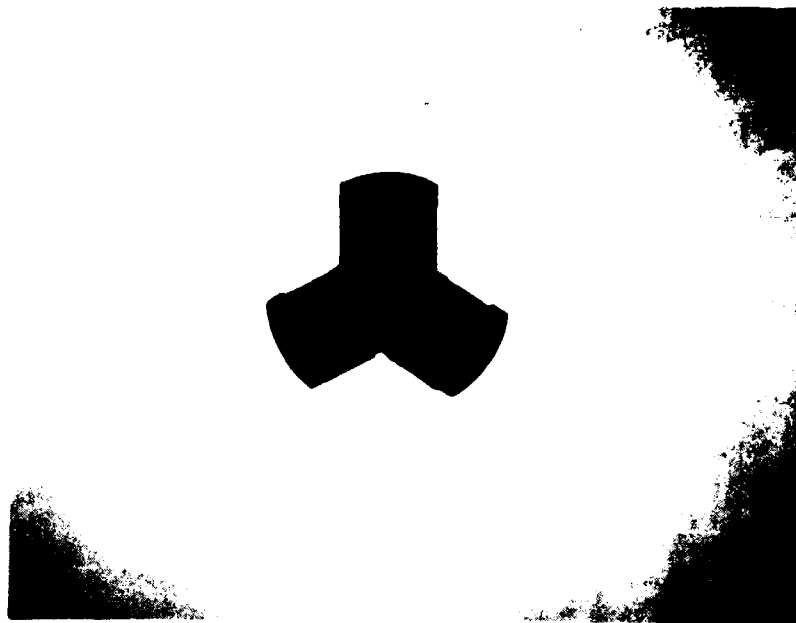


Figure 17. Three-Phase Core

For intermediate test, three side coils and center coils were checked for inductances and resistances. Unacceptable performance was corrected by rewinding the coils.

All the assemblies that passed intermediate tests were potted. Insulation on the ends of the wire were stripped and tips tinned for soldering to connectors. Figure 18 shows a potted three-phase eddy current probe. Potted three-phase probes then were lapped so that the pole face is flat against the specimen. Mating connectors were also wired for electrical connections.



Figure 18. Potted Three-Phase Probe

Quad Cup Probe

Fabrication of the quad cup probes were relatively simple. Commercially available ferrite cross cores were used. The center pole was machined off flush to the inside surface as shown in Figure 19. A plastic bobbin wound with 38 AWG magnet wire was bonded at the center of the inside of the core. Magnet wire of 36 AWG was used to wind the four legs of the core. The legs opposite each other were under one continuous winding. Therefore,

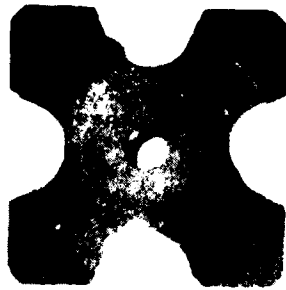


Figure 19. Quad Cup Core

there were only three independent coils in the quad cup probe, i.e., two driving coils and one detection air coil at the center. Electrical parameters were checked during the intermediate test similar to that of three-phase coils. Final assembly consisted of bonding of the quad cup probe to a plexiglass support and adding mating connectors for electrical connections. An assembled quad cup probe is shown in Figure 20.

4.2 Sample Configuration

Ten GFM specimens provided by AFWAL are shown in Appendix A, Figures A-1 to A-10. In all figures the top photo shows the inner layer structure and the bottom photo shows the outer layer surface. Each consisted of from one to three layers of aluminum fastened to one another. Notching of these specimens, in accordance with the approved plan, is shown in Appendix B, Tables B-1 to B-10.

The Government Furnished Material (GFM) consisted of sections cut out of C5A and C141 aircraft. These specimens were removed from various locations of the wings and were generally 2 to 4 feet in length and 6 to 12 inches in width. In order to notch these specimens, each section had to be disassembled

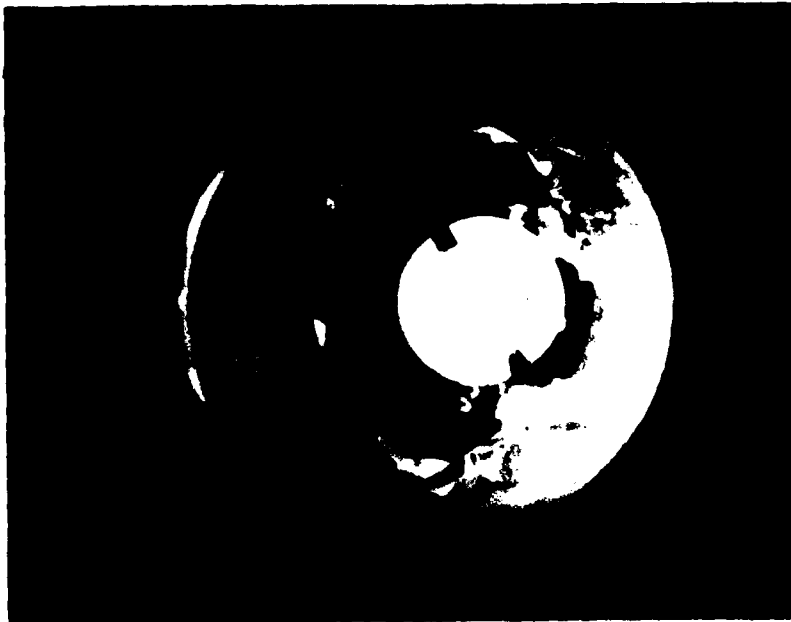


Figure 20. Quad Cup Probe

in order to put a through slot in the second layer. Jeweler's saw blades that do not exceed 0.008 inch in thickness were used to accomplish this task. After the notching process, care was taken to ensure that no metal particle was left in the bolt hole area, and that paint or coating on the surface was not disturbed. The parts were then reassembled with the original fasteners.

Eleven simulated C5 wing structures were also fabricated for calibration and testing. Simulated structure coupons were cut from 0.25-inch 7075-T6 aluminum sheet. The bolt holes on the top surfaces were countersunk at 100 degrees to accommodate standard shear type Hilock titanium fasteners. Each coupon was bolted together with titanium fasteners. Their configurations are shown in Figures 21 through 23, and a list of the specimens is shown in Table 1.

Sealant condition was simulated by the coupons adhered together with strips of plastic tape coated with adhesive on both sides. Thickness of the tape was approximately 0.003 inch thick.

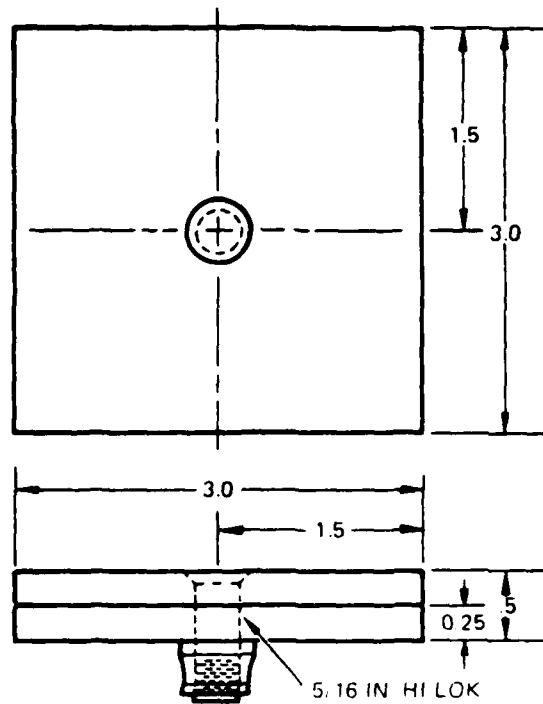


Figure 21. Simulated C-5A Specimen (Type I)

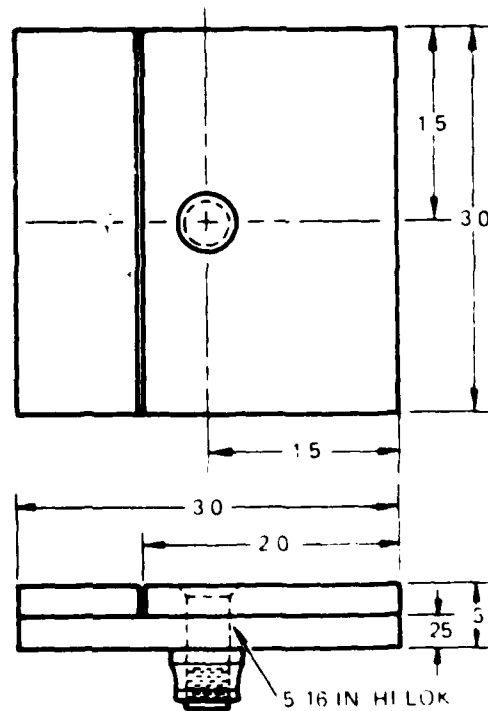


Figure 22. Simulated C-5A Specimen (Type II)

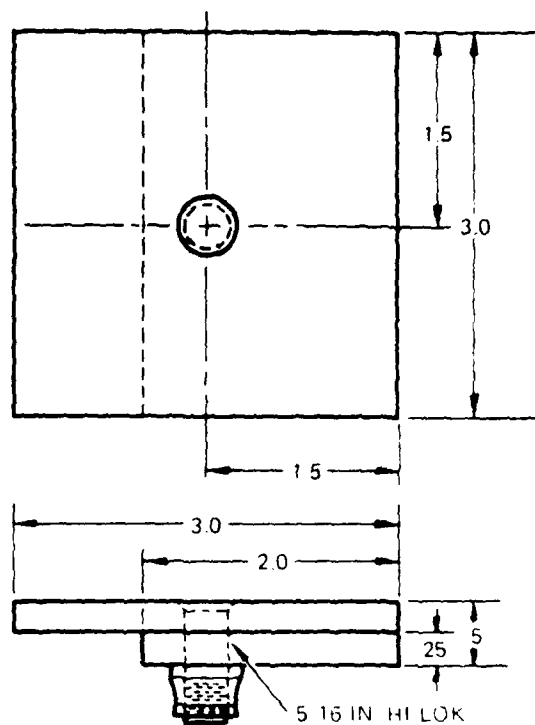


Figure 23. Simulated C-5A Specimen (Type III)

TABLE 1. SIMULATED C-5A SPECIMEN LIST

SPECIMEN NO.	TYPE	SLOT LENGTH (INCH)
1	I	0-No Flaw
2	I	0.15
3	I	0.10
4	I	0.08
5	I	0.04
6	II	0-No Flaw
7(1)	II	0.10
8(2)	II	0.10
9	III	0-No Flaw
10(3)	III	0.10
11(4)	III	0.10

NOTE:

1. Notch toward splice.
2. Notch away from splice.
3. Notch toward edge.
4. Notch away from edge.

4.3 Flaw Detection Technique

Multisegment Probe

Figure 24 shows the computerized eddy current array scanning system. A Tektronix 4052 graphic minicomputer acts as the system controller and display unit. A Hewlett-Packard 3438A programmable digital voltmeter is used as an analog to digital converter (ADC). An Interstate 845 programmable function generator supplies the driving voltage to the center coil of the array probe. A multiplexer board is used as a switching network to scan the segment voltage output. The multiplexer diagram is shown in Figure 25. A General Purpose Interface Bus (GPIB) board is used to bring the multiplexer functions such as segment selection, scanning sequence and speed under computer control. Figure 26 shows the GPIB board wiring diagram. A signal expander expands ac voltage from the segment and converts the signal to dc level. Figure 27 shows the schematics of the signal expander. All data transfers are accomplished on the GPIB bus.

The commercial LFEC equipment interface was accomplished by replacing the function generator with the Alcoprobe instrument. A digital signal line was added from the GPIB board to the Alcoprobe input. It triggers the alarm when a preset threshold level is reached. The system driving signal is supplied by the Alcoprobe output and a power amplifier was added to boost the driving voltage. A block diagram of the interface is shown in Figure 28. With the exception of above minor modifications, the system configuration is essentially unchanged as compared to Figure 24.

Centering of the bolt hole was accomplished by a Maxwell bridge circuit, a null detector, and a second function generator operated at 20KHz as shown in Figure 29. The same center driving coil used for crack detection was used for centering purposes. If the probe was centered over the fastener hole, the bridge would be in a balanced state, and the null detector would show no error voltage due to the symmetrical geometry of the fastener head. If the probe was off center, it would cause the bridge to unbalance and would be indicated by the null detector. Figure 30 shows the schematics of a mechanical switch box layout. The box switches between centering frequency, f_c , and normal detecting operating frequency, f_o . This set-up enabled the multisegment probe to be used as both a centering and a detecting device without any cable connect and disconnect required.

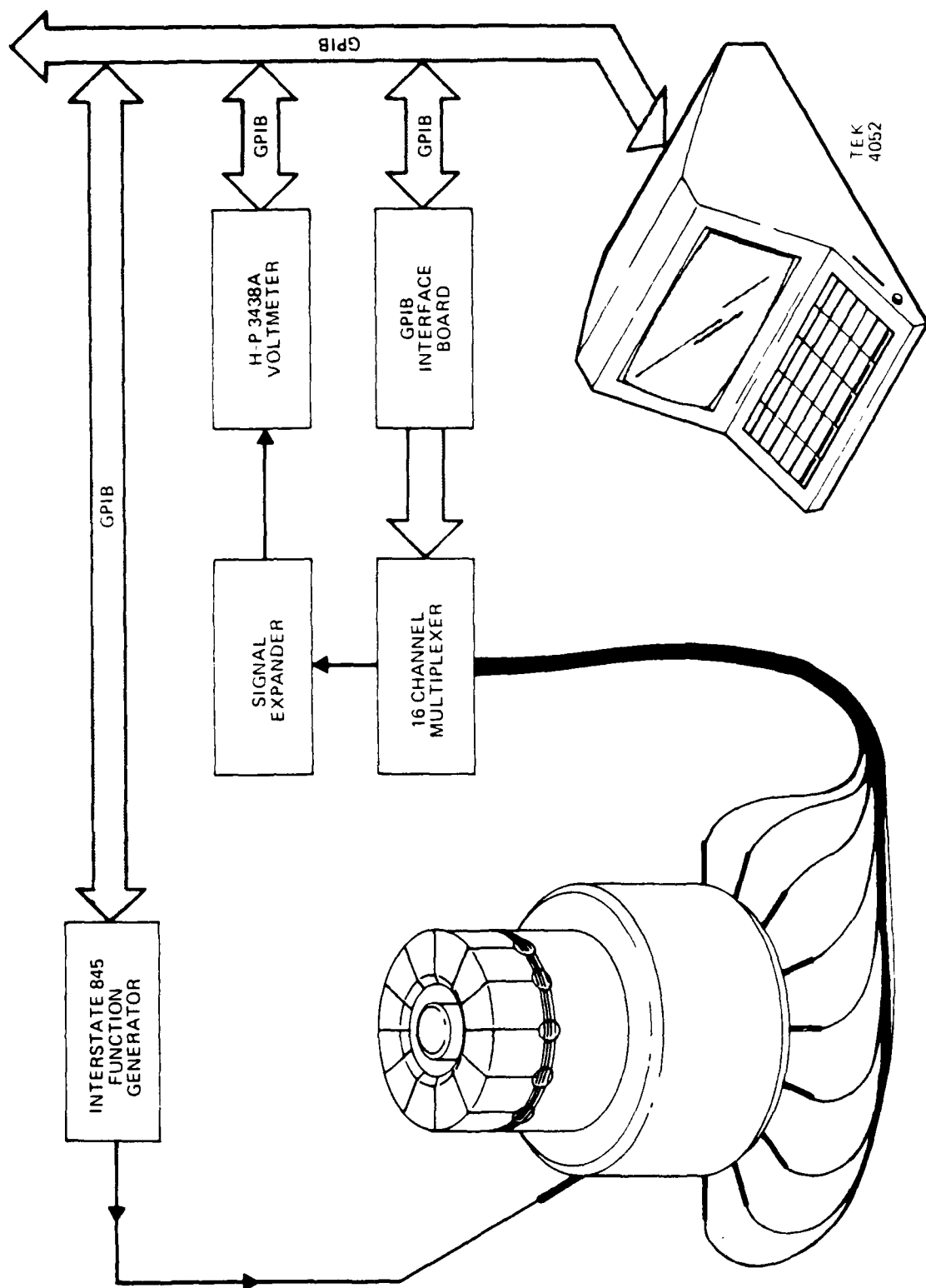
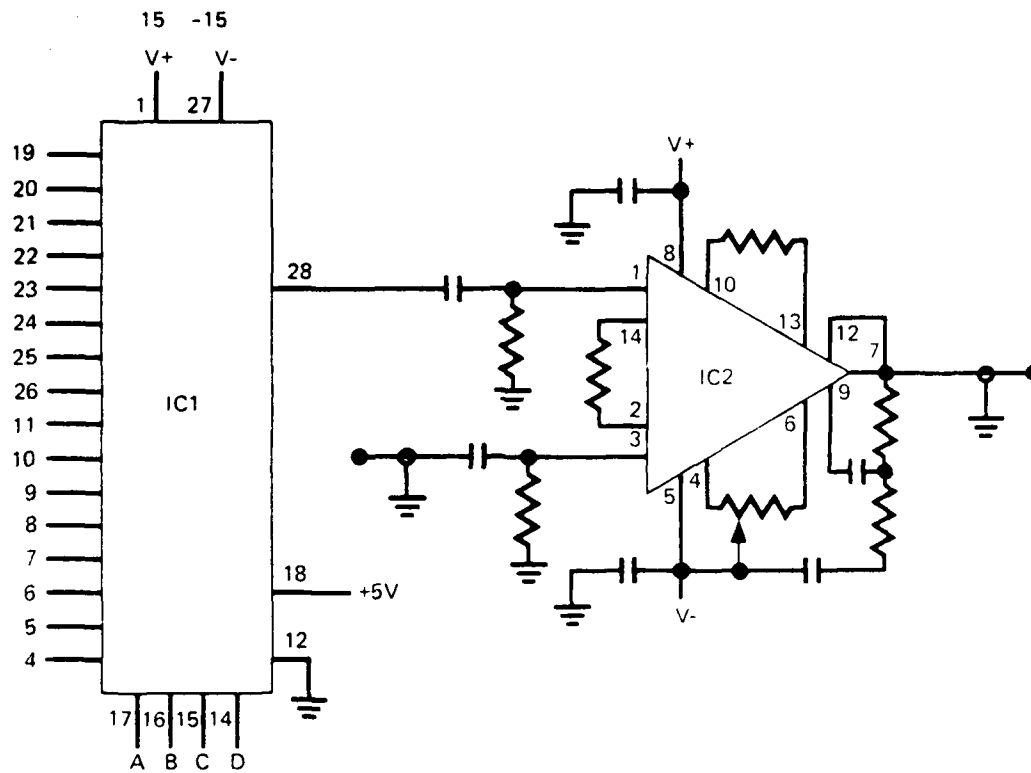


Figure 24. Computerized Eddy Current Scanning System



IC1 16 CHANNEL MULTIPLEXER
IC2 INSTRUMENTATION AMPLIFIER

Figure 25. Probe Segments Scanning Scheme

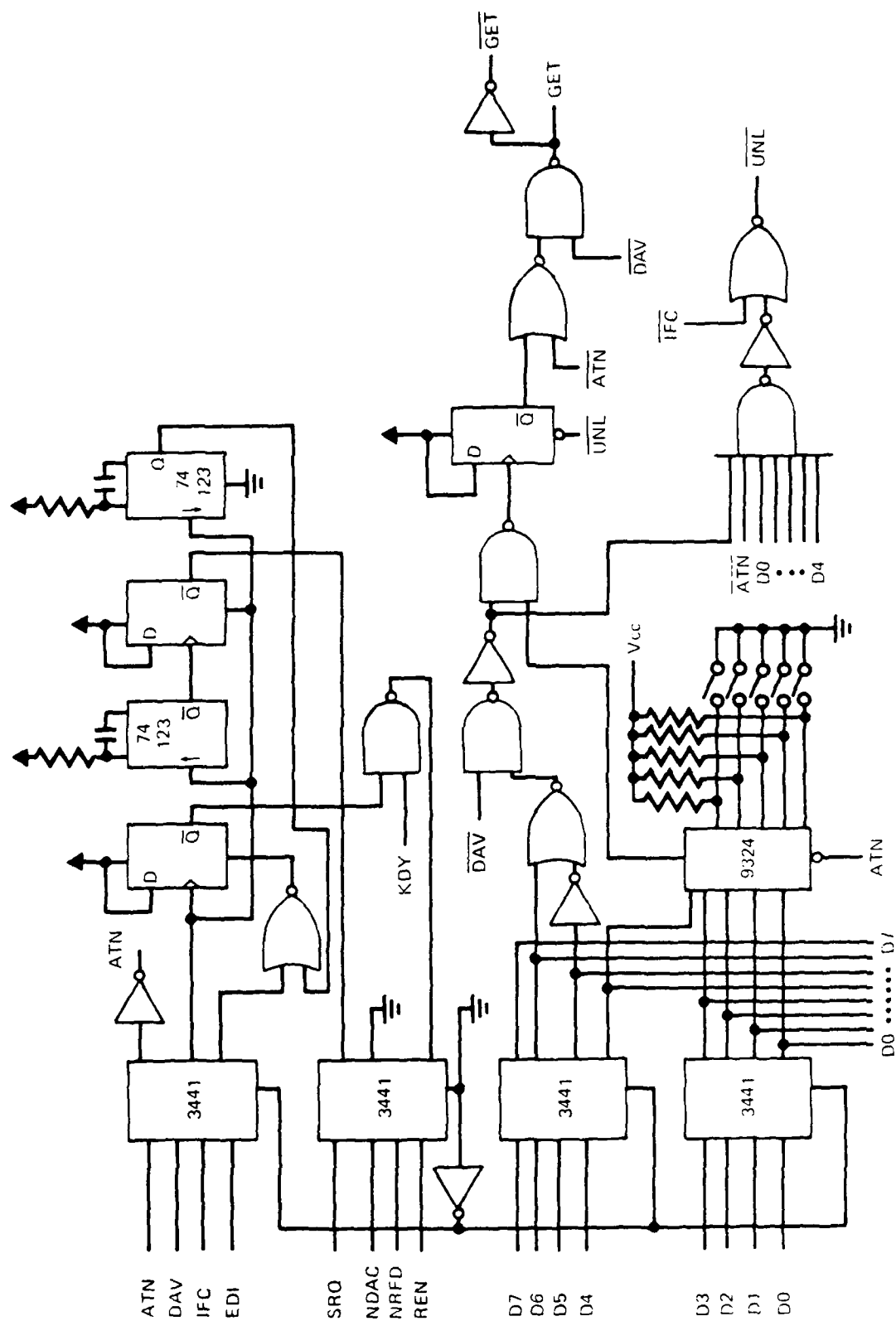


Figure 26. GPIB Interface Wiring Diagram

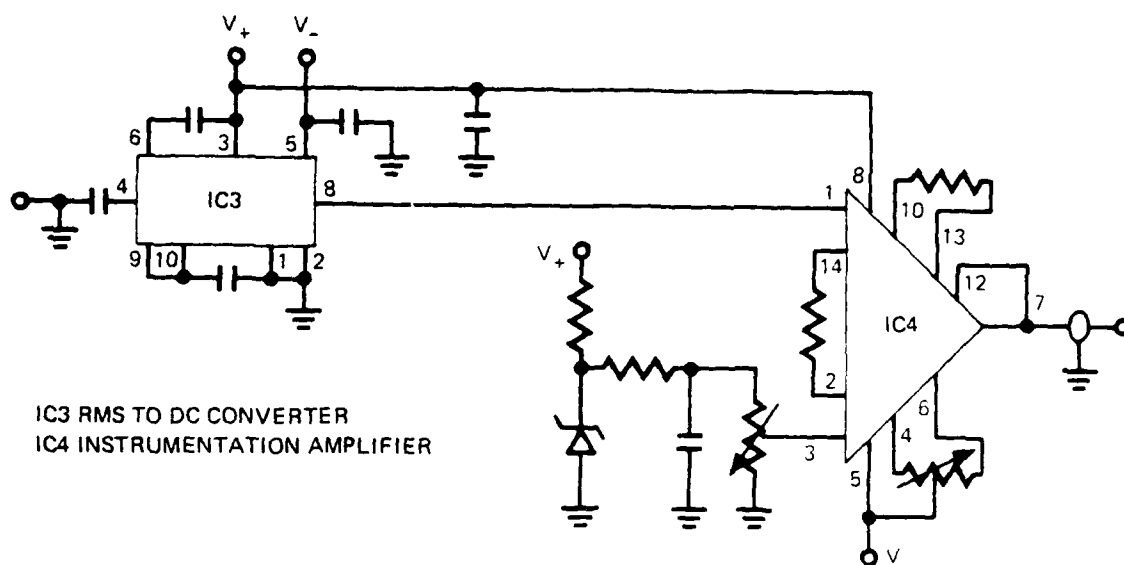


Figure 27. Signal Expander / Level Shifter

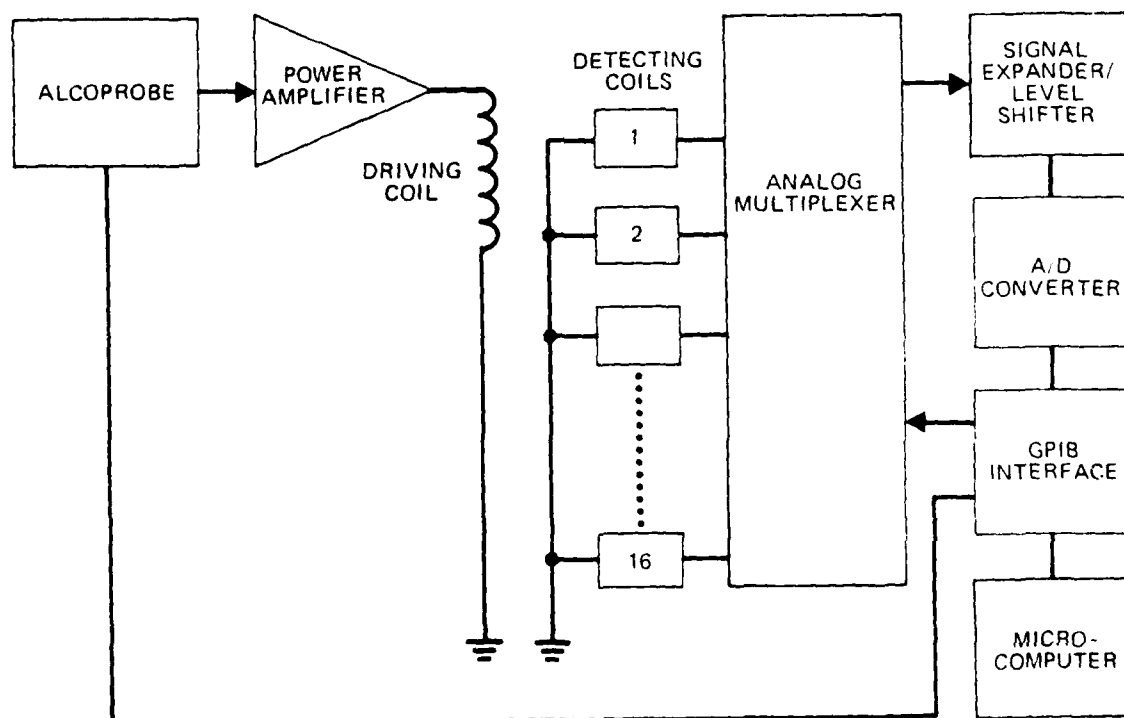


Figure 28. Commercial Instrument Interface Diagram

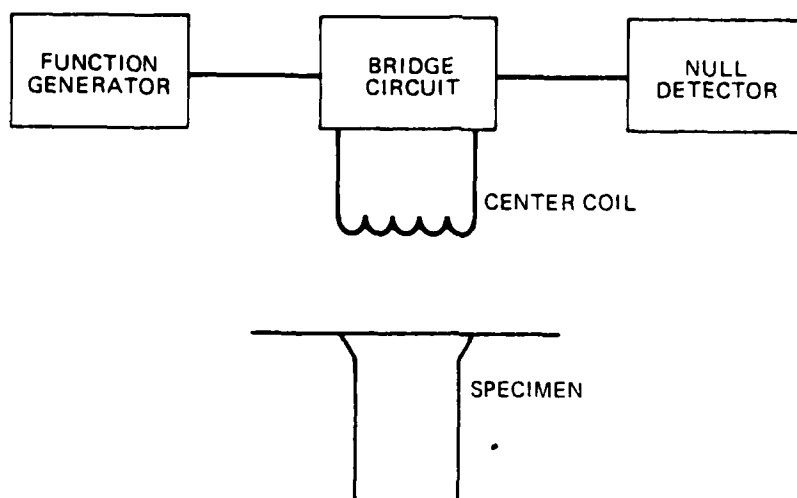


Figure 29. Centering Block Diagram

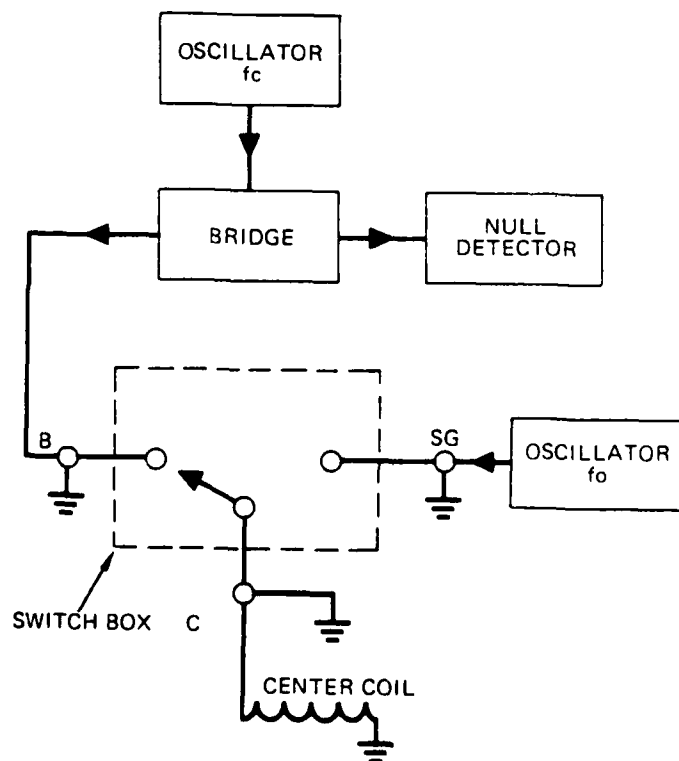


Figure 30. Electronic Centering Schematics

The crack detection steps are as follows:

1. An unflawed specimen is placed on the array probe as a reference standard. When the probe is centered over the standard as described previously, the computer triggers the function generator for a preprogrammed signal with desired frequency and amplitude. The signal is supplied to the center driving coil. Induced eddy current signals are then picked up by the segment coils, scanned by the multiplexer, digitized by the voltmeter and stored in the computer as a numerical array. Each segment voltage is sampled several times to obtain an average reading.
2. The unflawed standard is removed from the probe and replaced by an unknown specimen. The centering and signal processing sequence repeats and stores the segment voltage readings in the computer as a second array.
3. The computer calculates the difference between the two array values and displays the asymmetry in graphic waveform. This information would be used to trigger an audio response in a commercial LFEC instrument if a crack is present.
4. Repeat step number 2 for subsequent specimens.

The laboratory apparatus set-up for second layer crack detection is shown in Figure 31. Figure 32 shows the hand-held probe for fastener hole inspection.

Three-Phase Probe

The mode of operation for a three-phase probe is the same as the classic three-phase drive used in AC motors to obtain a rotating magnetic field. In the case of crack detection, the center common sense coil was used to accurately center the probe over the fastener using a high frequency. The outer coils were driven in three-phase to rotate the field and eddy current around the bolt hole. Due to the center coil construction, the net error voltage resulting from the drive coils was zero because of the vector sum of three contributions. A slight adjustment of the drive voltages was used to adjust error voltage to zero to compensate for any fabrication asymmetries in the coils. The flux induced by the eddy current would be perfectly

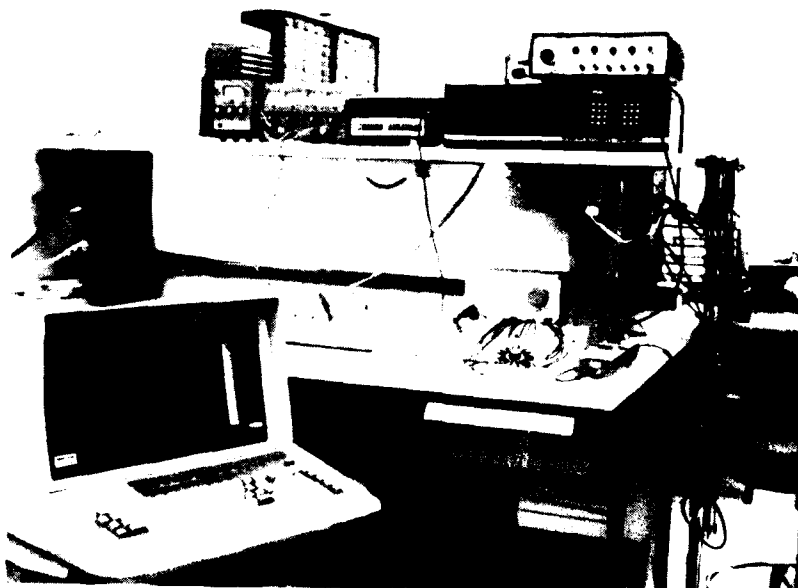


Figure 31. Laboratory Crack Detection Set-Up

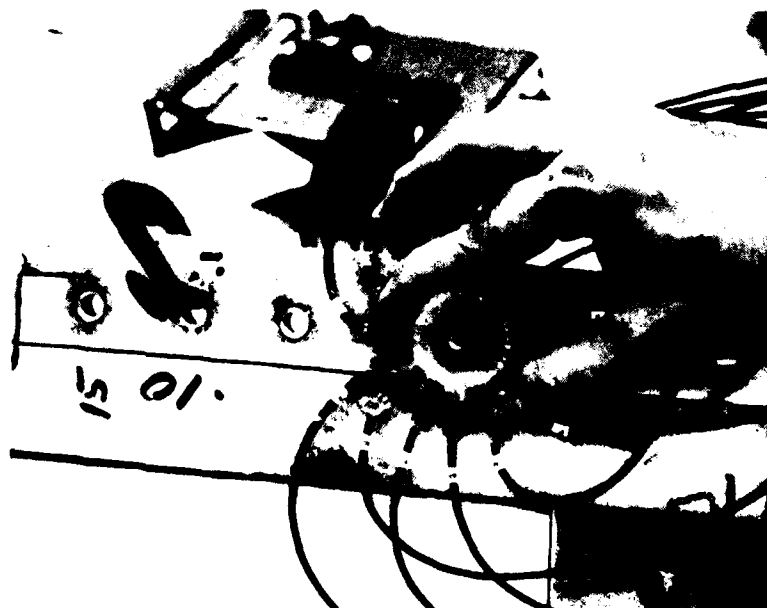


Figure 32. Hand-Held Inspection of GFM

symmetric and resulted in zero error voltage. Therefore, any asymmetry due to a flaw would cause a finite error voltage output.

Quad Cup Probe

Operation of the quad cup core was very similar to that of the three-phase probe, except that the applied fluxes are centered with respect to the fastener hole. The center air coil was used for centering. Two outer coils were driven at 180 degrees apart to rotate the field, and the center coil was used to detect error voltage due to a flaw.

SECTION 5

EXPERIMENTAL RESULTS

Multisegment Probe

As described in Section 4.3, the operating mode for the multisegment probe was to drive the center coil at the frequency of interest and measure the open circuit voltage at the segments. These voltages were then recorded for a specimen without flaws and used as a reference for a flawed or unknown specimen. The differences were used to determine the presence of a flaw. By comparing the segment variations, the location of the flaw could also be determined.

Experimental data in this section were all obtained at 400 Hz with driving voltage at 7.5 volts or 15 volts peak to peak, unless noted otherwise. Refer to Table 1 and Figures 21, 22, and 23 for specimen configurations.

Two sets of data plots were generated. One was for the simulated C-5A specimens with adhesive tape between the aluminum layers; one was without the tape. Since there were no visible differences between the data, only the plots for the specimens with adhesive tape left in the layers were presented. All the data were taken with the titanium fastener in place.

Figure 33 shows the plot for an unflawed specimen vs an unflawed standard. Figure 34 shows specimen 2 with the notch at segment 6, and Figure 35 shows its polar representation. Figures 36 through 39 show detection plots of specimen 3 with the notch rotated from segment 7 to segment 4-5. Detection plots for specimens 4 and 5 are shown in Figures 40 and 41. Different frequencies were used on specimen 5 for crack detection. Figures 42, 43, 44, and 45 show detection responses at 300, 500, 600, and 700 Hz, respectively.

Skin splice coupons (Type II) were examined next. Figure 46 shows the plots of specimen 6 vs a no flaw skin splice coupon. Detection plot of specimen 7 is shown in Figure 47. Specimen 7 was reexamined by shifting the probe reference position one segment, or 22.5 degrees between the no flaw specimen and test

specimen and the result is shown in Figure 48. Segment offset experiment was also tried on specimen 8 and the result is shown in Figure 49, actual flaw is on segment 1.

Structural edge coupons (Type III) were examined also. Figure 50 shows the plot of specimen 9 vs a no flaw structural edge coupon. Detection plot for specimen 10 is shown in Figure 51. Specimen 10 was reexamined by one segment offset between no flaw reference mode and test mode, and the result is shown in Figure 52. Figure 53 shows the detection plot of specimen 11 shifted by one segment, actual flaw is on segment 1.

Figure 54 is a graph of raw data of Type I specimens. Absolute segment voltages were plotted against each other.

Flaw detection on the GFM was performed primarily on the pieces with 0.3125-inch diameter holes. Baseline data were collected from no flaw fastener holes adjacent to the flawed holes to minimize the boundary effect in the surrounding area. Figures 55 through 61 show the detection plots for GFM specimens A, E, and I.

Attempts on outer layer flaw detection have also been tried with the same multisegment probes. Typical data are shown in Figure 62. Slot length is 0.02 inch and located underneath the countersink. Operating frequency was 1.5 KHz at 8 volts.

Three-Phase Probe

The three-phase probe failed to detect any flaw in any of the simulated specimens. The probe output gave small flaw indication only when the 0.25 inch first layers were replaced by 0.08 inch first layers for specimens 2 and 3. The flaw indication was in the form of meter movement. Therefore, graphic display could not be obtained.

Quad Cup Probe

The quad cup probe had slight success only with specimens 2 and 3, but the notch must be under one of the legs. The probe required a 90 degree mechanical rotation around the fastener in order to make a complete inspection. The crack indication was also in the form of meter movement.

CRACK DETECTION UNDER INSTALLED FASTENER (T1)

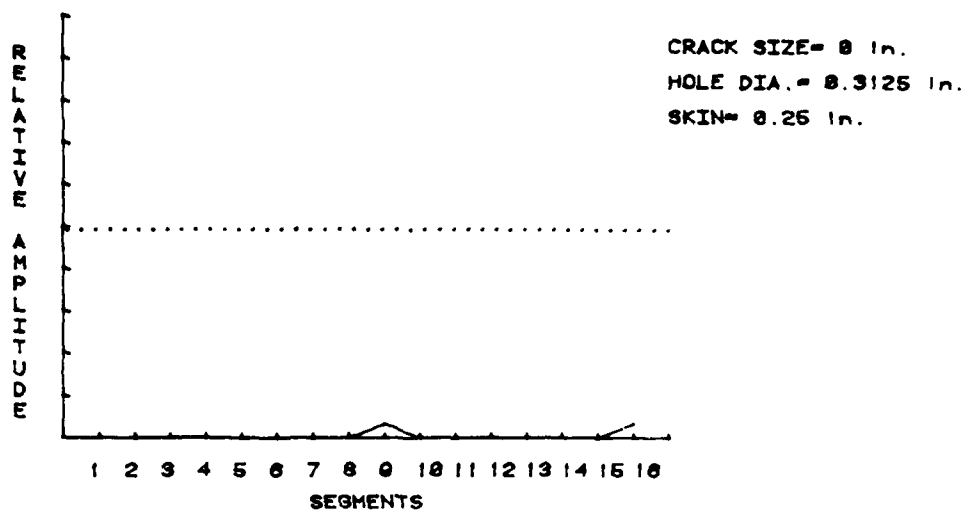


Figure 33. Detection Plot of Specimen 1

CRACK DETECTION UNDER INSTALLED FASTENER (T1)

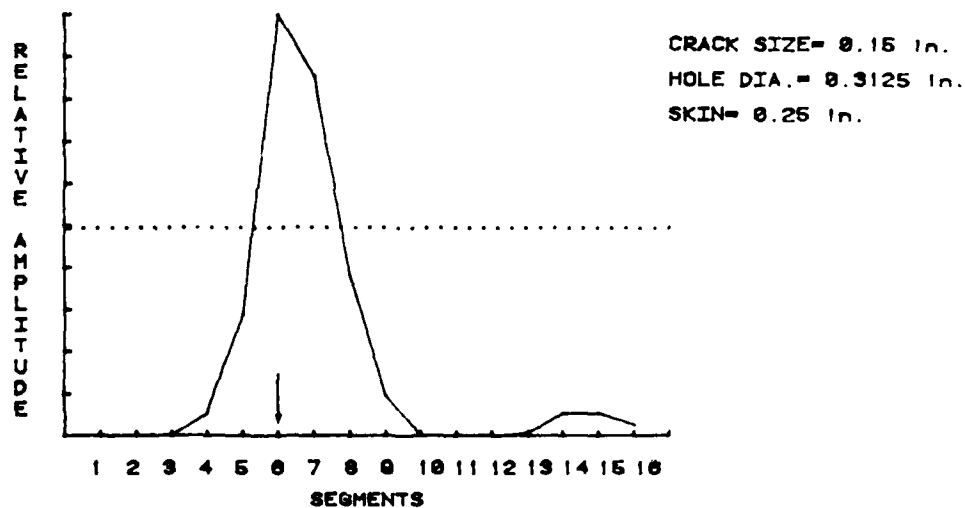


Figure 34. Linear Plot of Specimen 2

CRACK DETECTION UNDER INSTALLED FASTENER (T1)

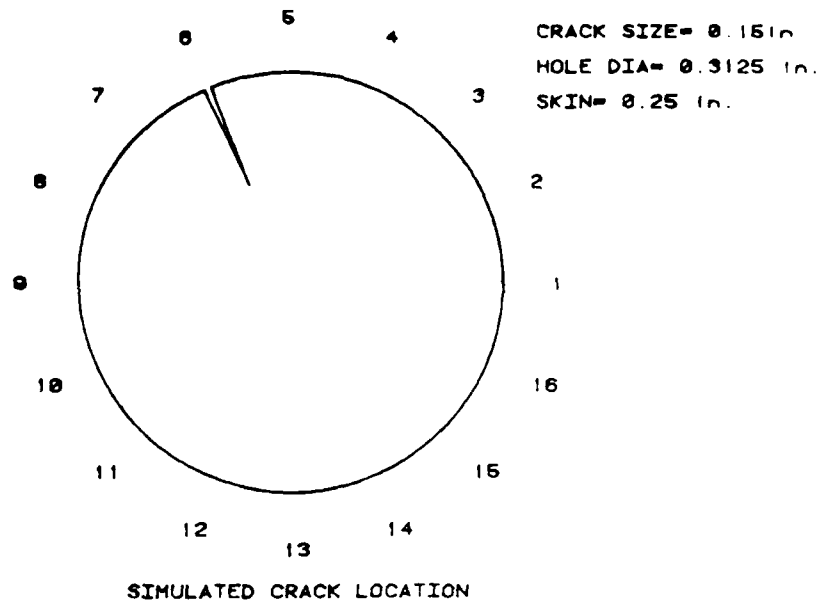


Figure 35. Polar Plot of Specimen 2

CRACK DETECTION UNDER INSTALLED FASTENER (T1)

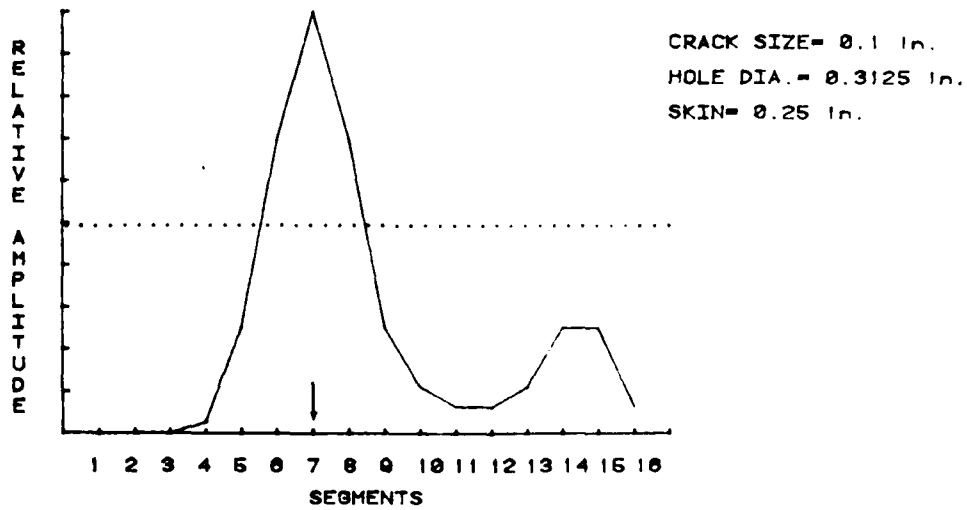


Figure 36. Linear Plot of Specimen 3

CRACK DETECTION UNDER INSTALLED FASTENER (T1)

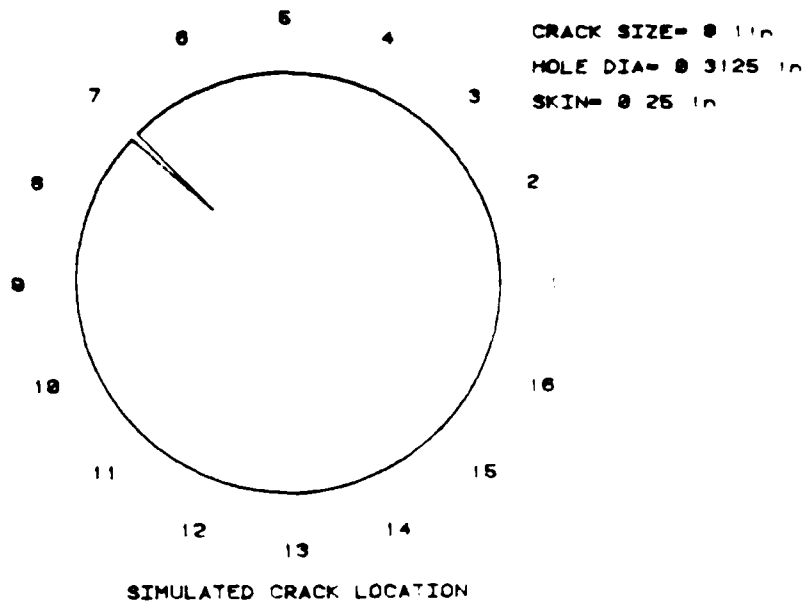


Figure 37. Polar Plot of Specimen 3

CRACK DETECTION UNDER INSTALLED FASTENER (T1)

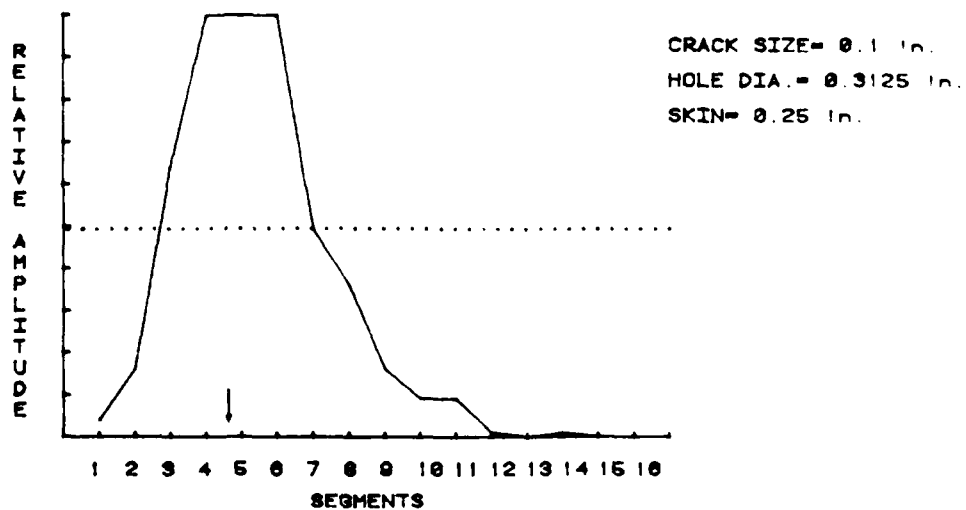


Figure 38. Linear Plot of Specimen 3

CRACK DETECTION UNDER INSTALLED FASTENER (T1)

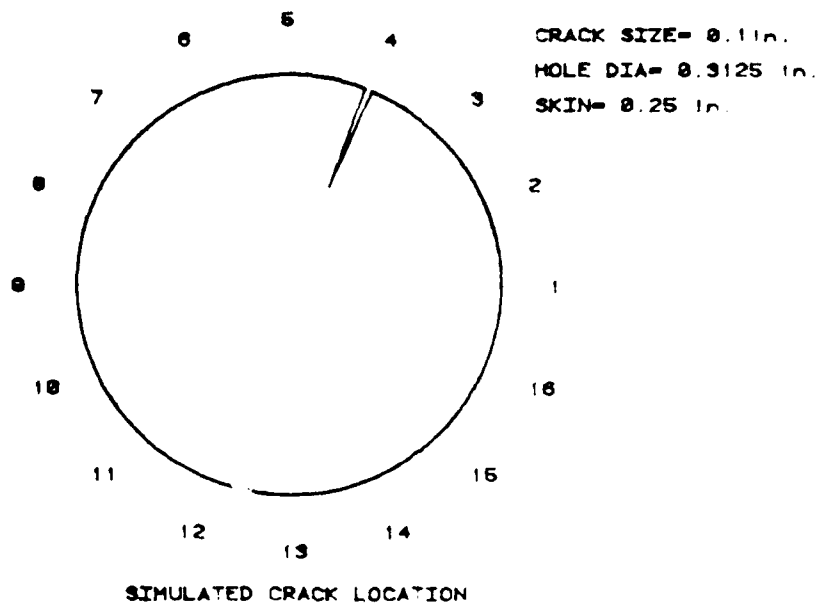


Figure 39 Polar Plot of Specimen 3

CRACK DETECTION UNDER INSTALLED FASTENER (T1)

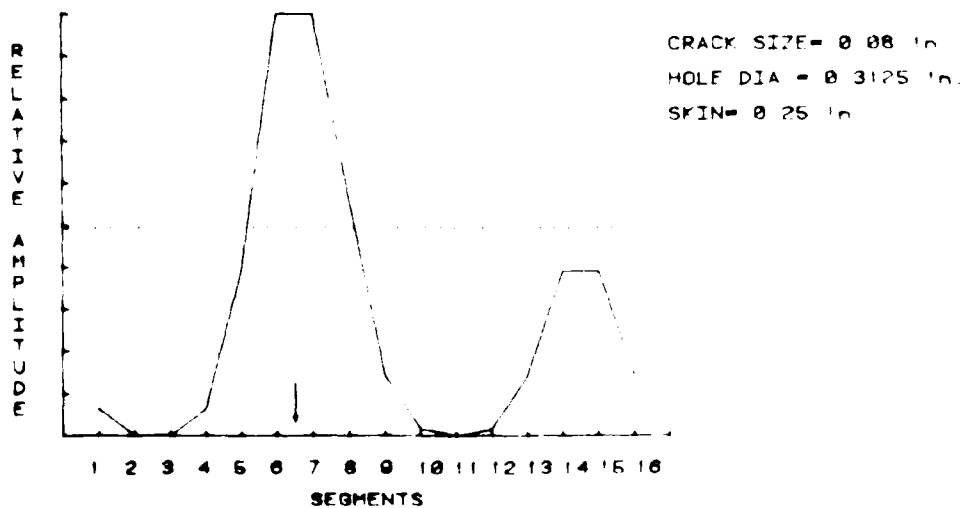


Figure 40 Detection Plot of Specimen 4

CRACK DETECTION UNDER INSTALLED FASTENER (T1)

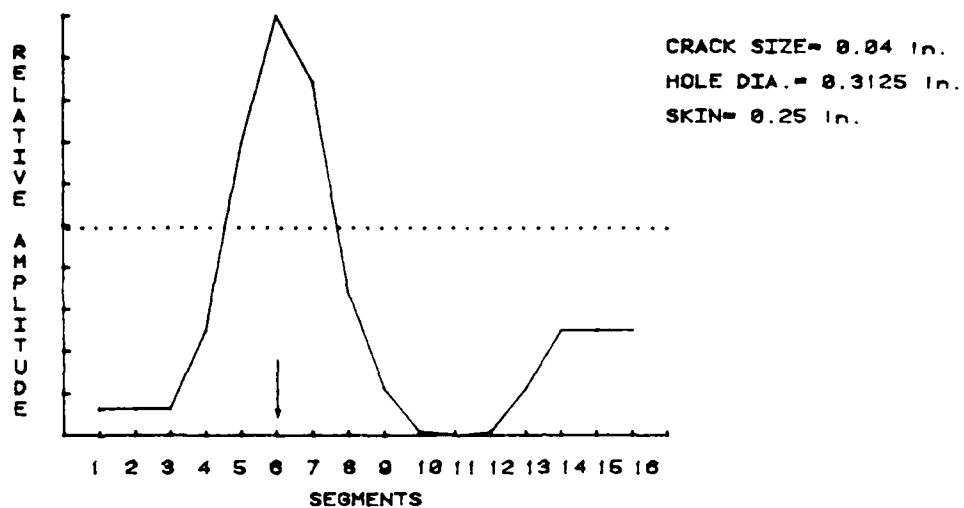


Figure 41. Detection Plot of Specimen 5

CRACK DETECTION UNDER INSTALLED FASTENER (T1)

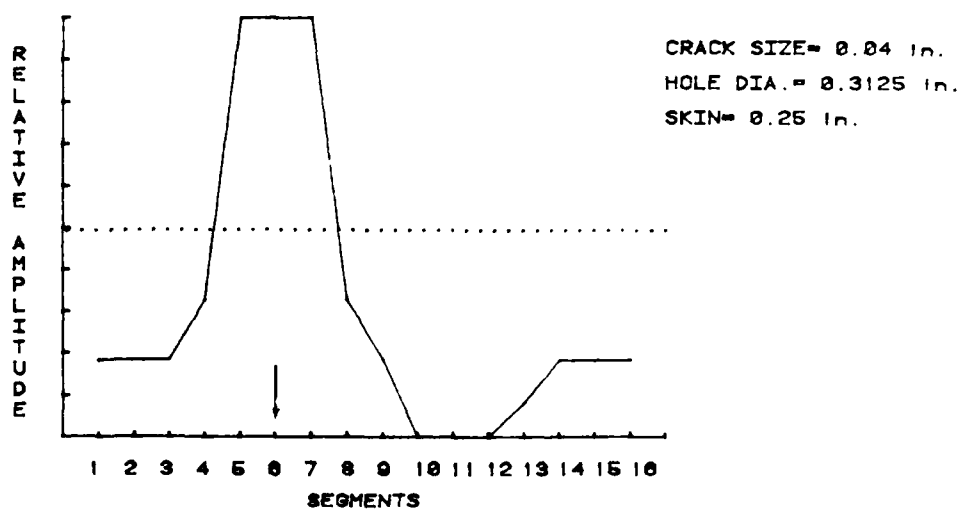


Figure 42. Detection Plot of Specimen 5 at 300 Hz.

CRACK DETECTION UNDER INSTALLED FASTENER (T1)

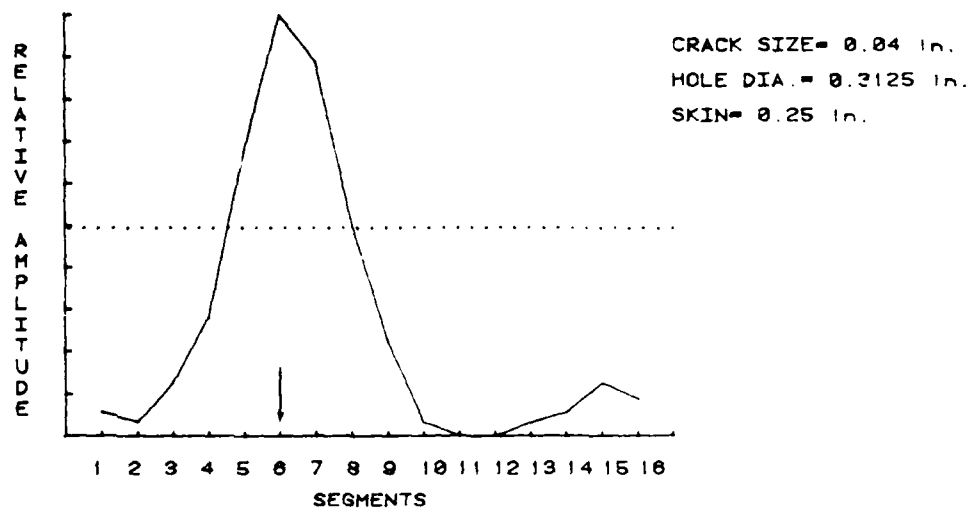


Figure 43. Detection Plot of Specimen 5 at 500 Hz.

CRACK DETECTION UNDER INSTALLED FASTENER (T1)

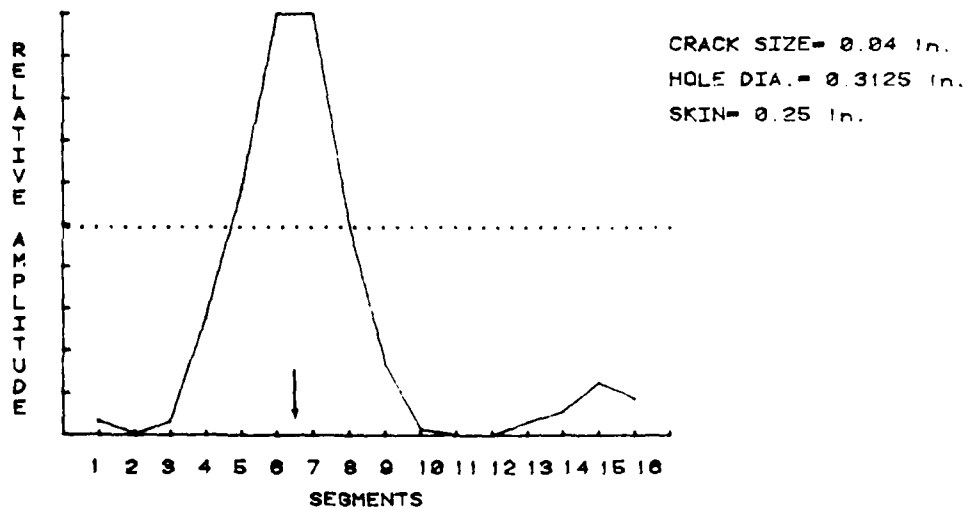


Figure 44. Detection Plot of Specimen 5 at 600 Hz.

CRACK DETECTION UNDER INSTALLED FASTENER (T1)

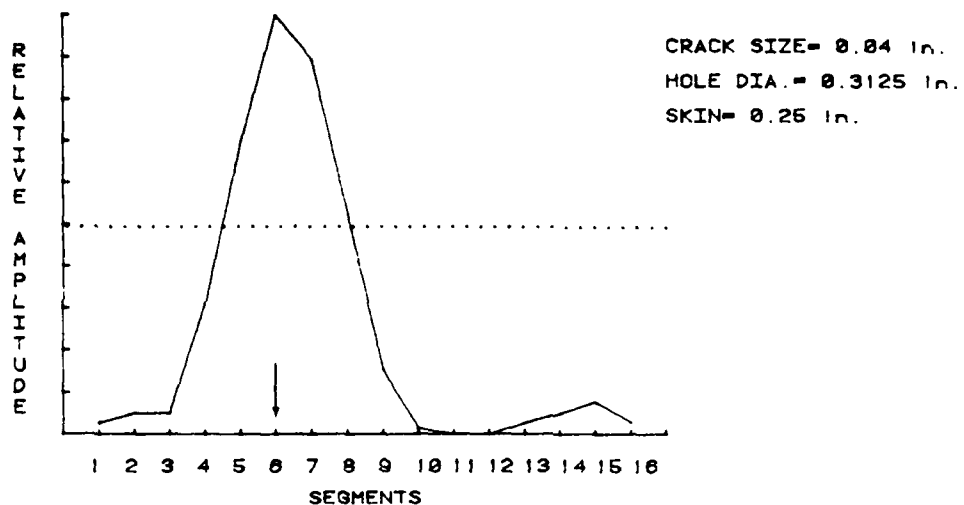


Figure 45. Detection Plot of Specimen 5 at 700 Hz.

CRACK DETECTION UNDER INSTALLED FASTENER (T1)

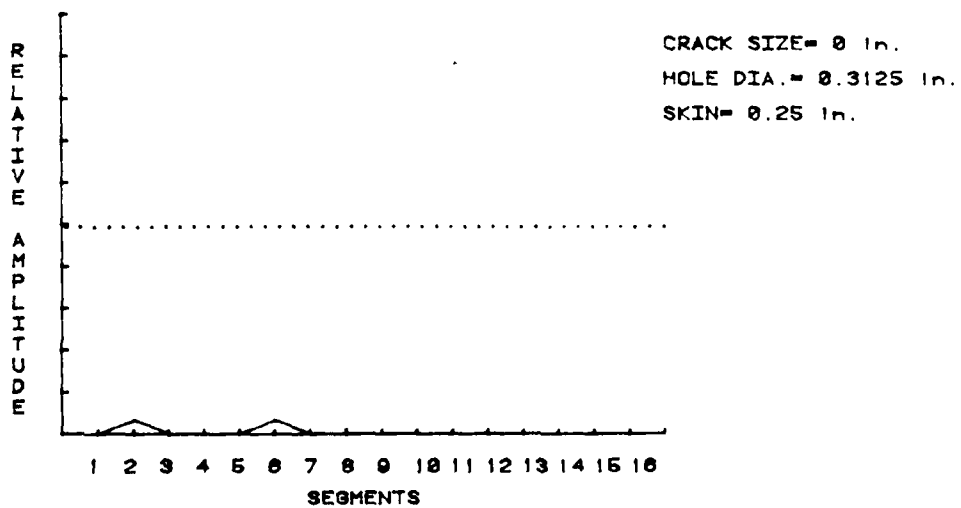


Figure 46. Detection Plot of Specimen 6

CRACK DETECTION UNDER INSTALLED FASTENER (T1)

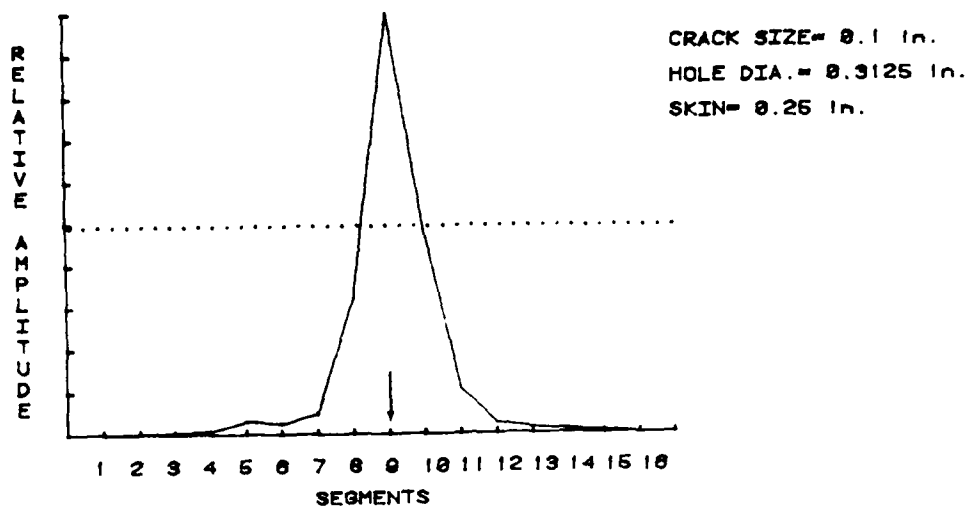


Figure 47. Detection Plot of Specimen 7

CRACK DETECTION UNDER INSTALLED FASTENER (T1)

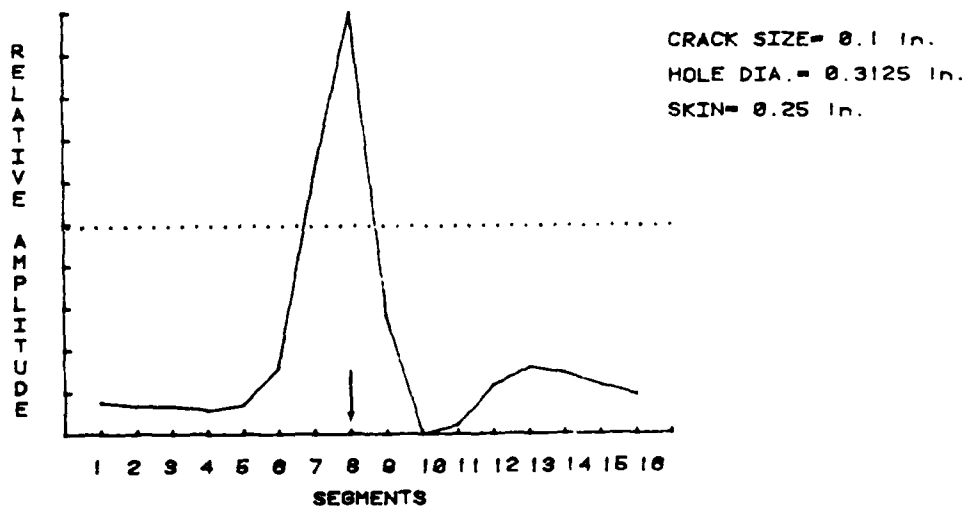


Figure 48. Detection Plot of Specimen 7
with One Segment Offset

CRACK DETECTION UNDER INSTALLED FASTENER (T1)

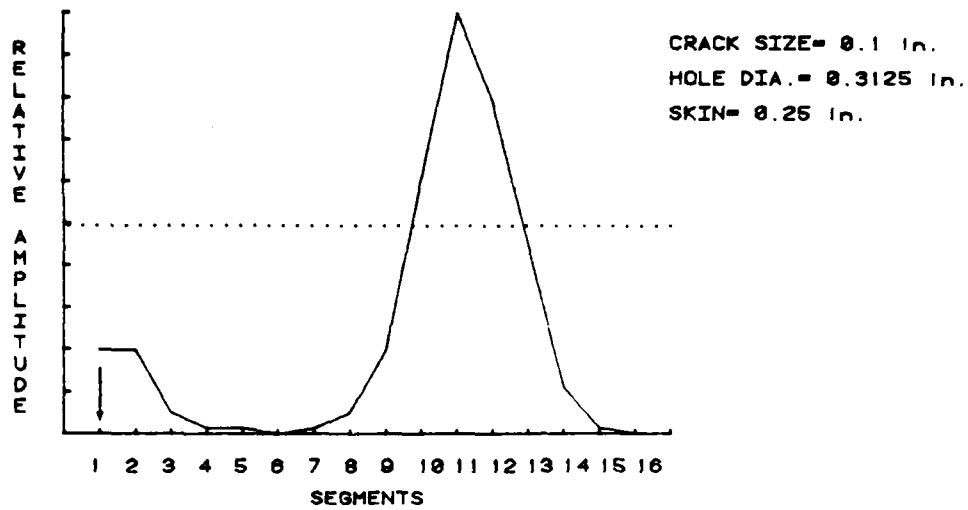


Figure 49. Detection of Specimen 8 with One Segment Offset

CRACK DETECTION UNDER INSTALLED FASTENER (T1)

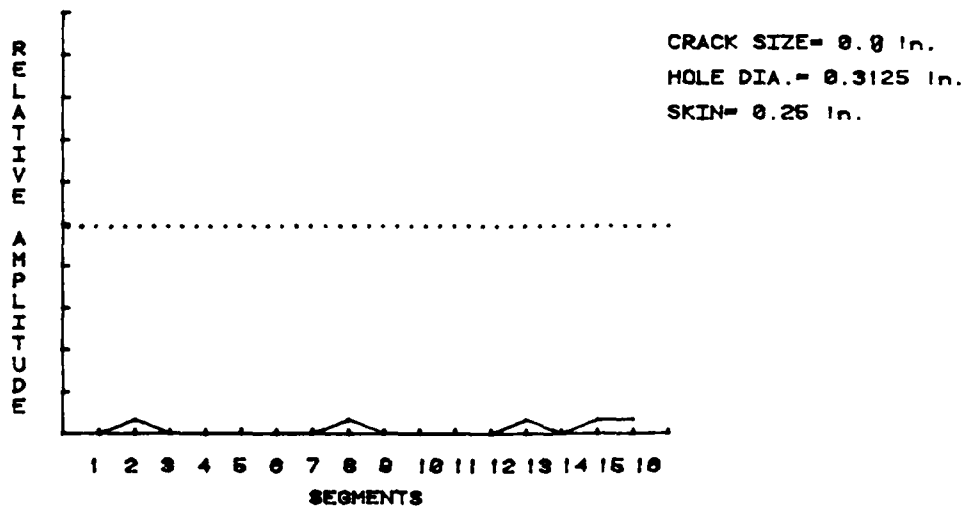


Figure 50. Detection Plot of Specimen 9

CRACK DETECTION UNDER INSTALLED FASTENER (T1)

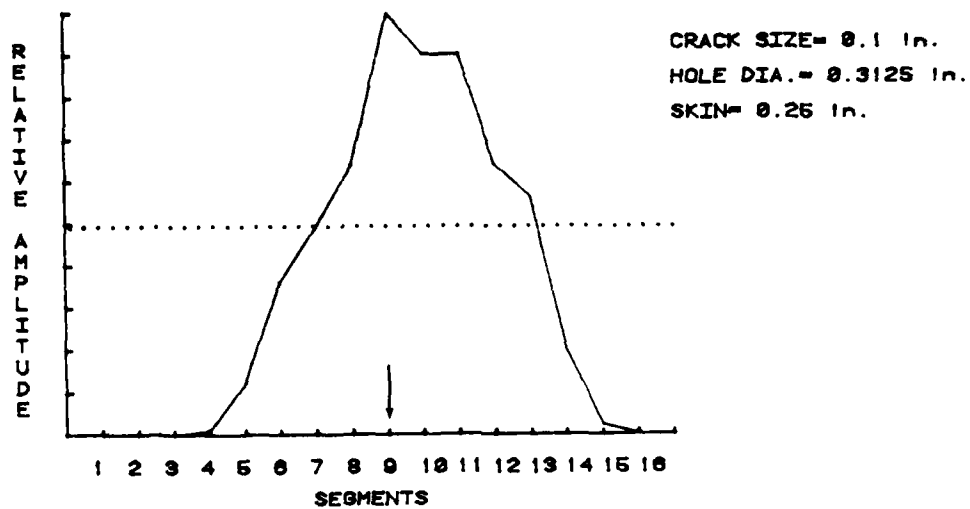


Figure 51. Detection Plot of Specimen 10

CRACK DETECTION UNDER INSTALLED FASTENER (T1)

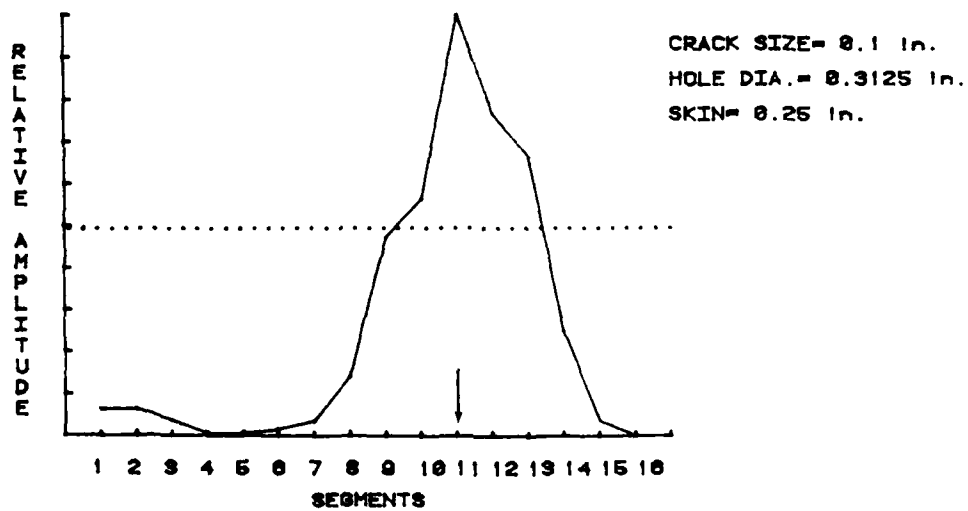


Figure 52. Detection Plot of Specimen 10
with One Segment Offset

CRACK DETECTION UNDER INSTALLED FASTENER (T1)

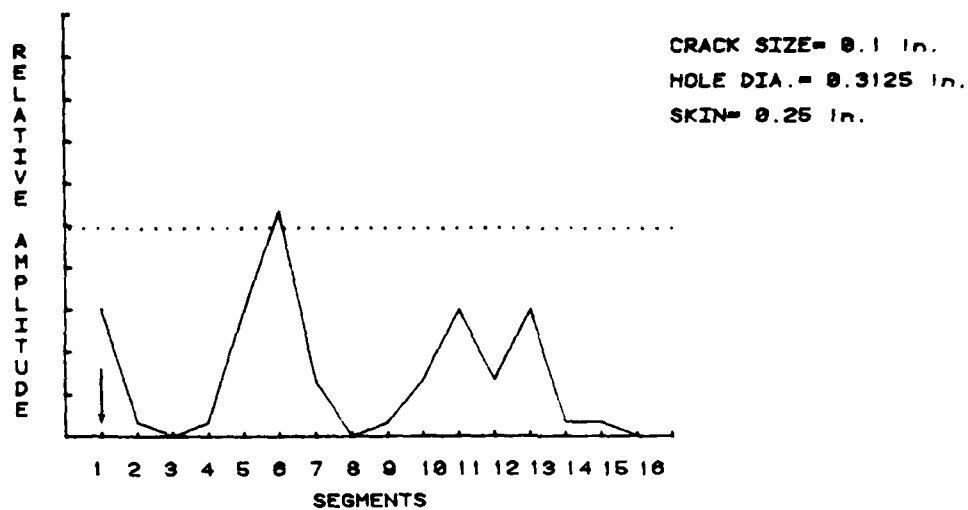


Figure 53. Detection Plot of Specimen 11

RESPONSE OF DIFFERENT FLAW LENGTH

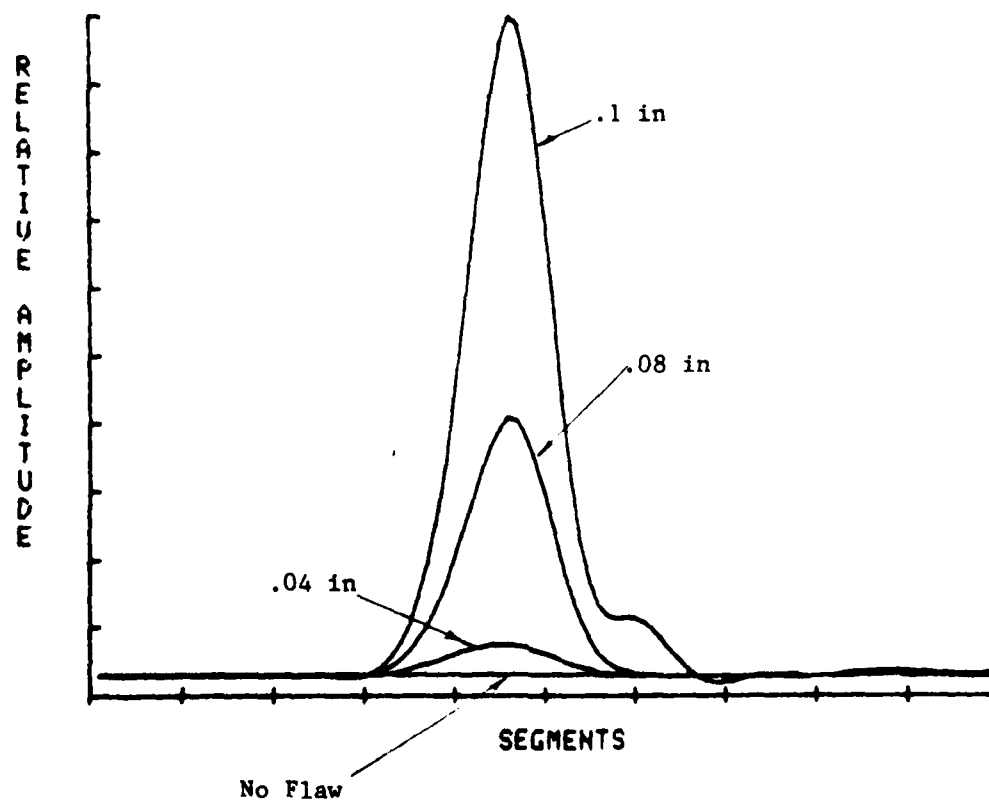


Figure 54. Relative Segment Voltages for Type I Specimens

CRACK DETECTION UNDER INSTALLED FASTENER (T1)

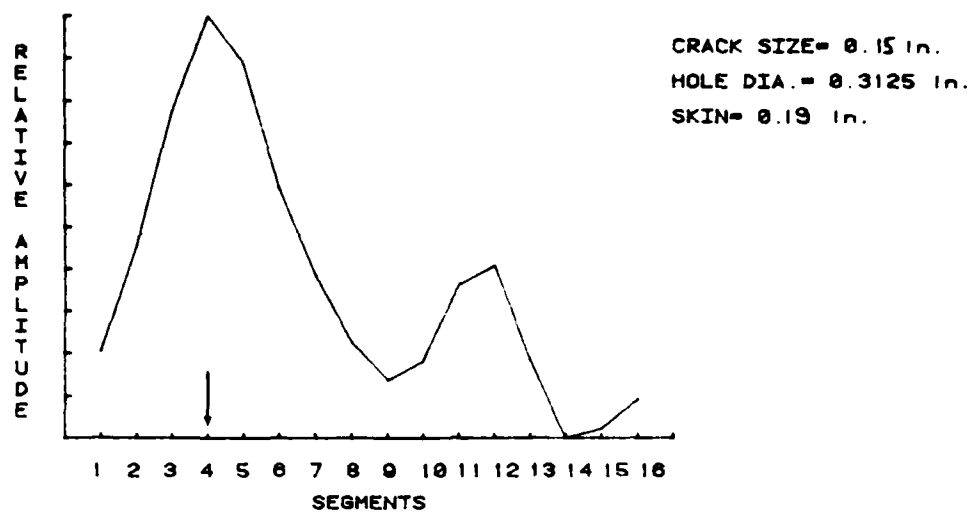


Figure 55. Detection Plot of GFM "Specimen A", Hole 2

CRACK DETECTION UNDER INSTALLED FASTENER (T1)

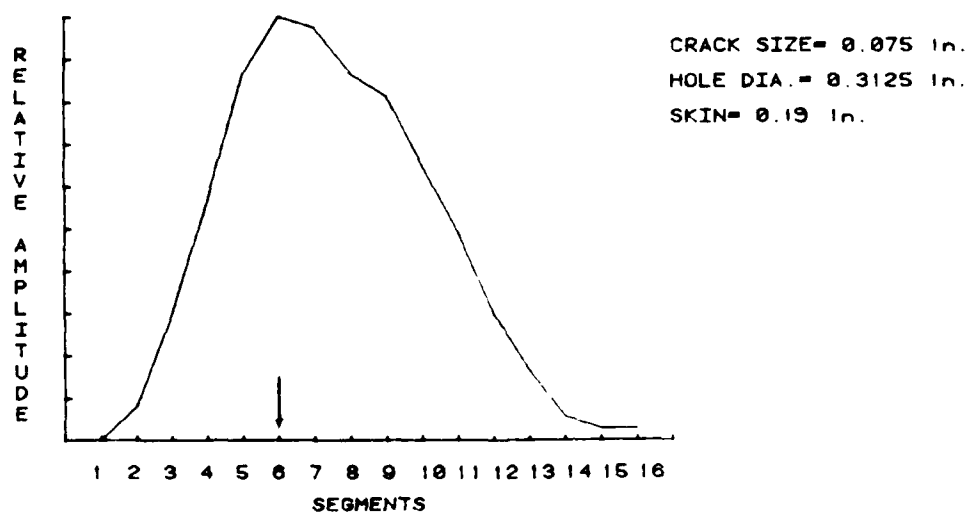


Figure 56. Detection Plot of GFM "Specimen A", Hole 11

CRACK DETECTION UNDER INSTALLED FASTENER (T1)

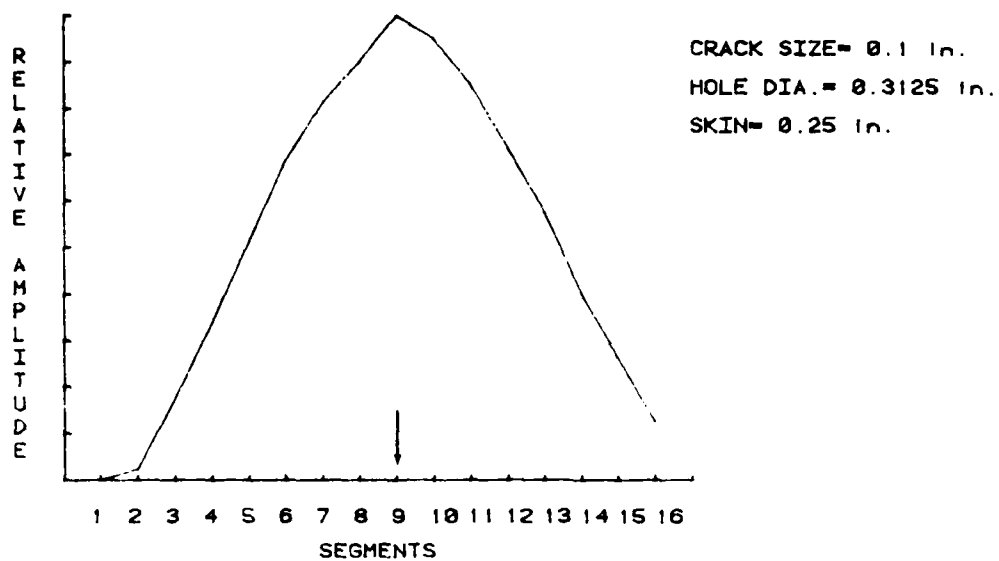


Figure 57. Detection Plot of GFM "Specimen E", Hole 8

CRACK DETECTION UNDER INSTALLED FASTENER (T1)

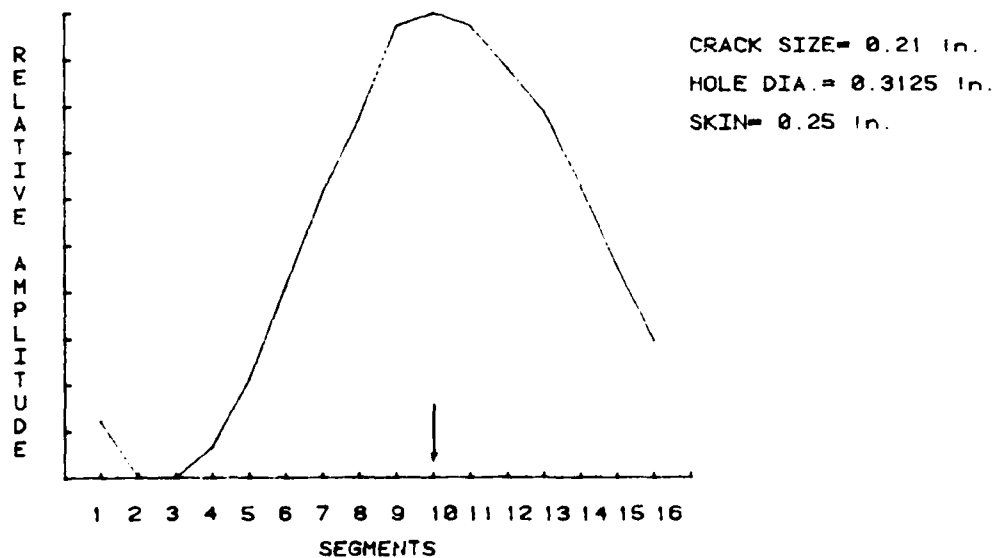


Figure 58. Detection Plot of GFM "Specimen E", Hole 10

CRACK DETECTION UNDER INSTALLED FASTENER (Ti)

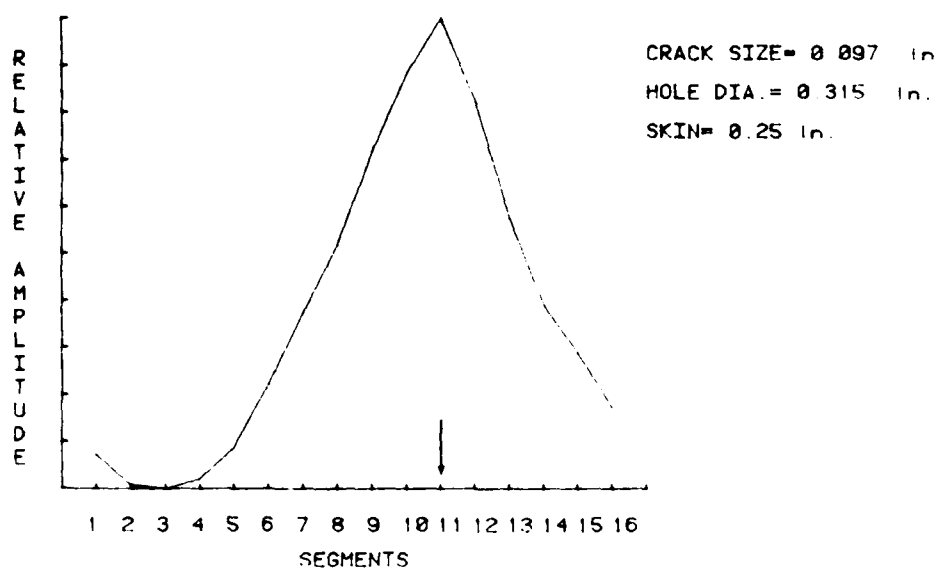


Figure 59. Detection Plot of GFM 'Specimen I', Hole 10

CRACK DETECTION UNDER INSTALLED FASTENER (Ti)

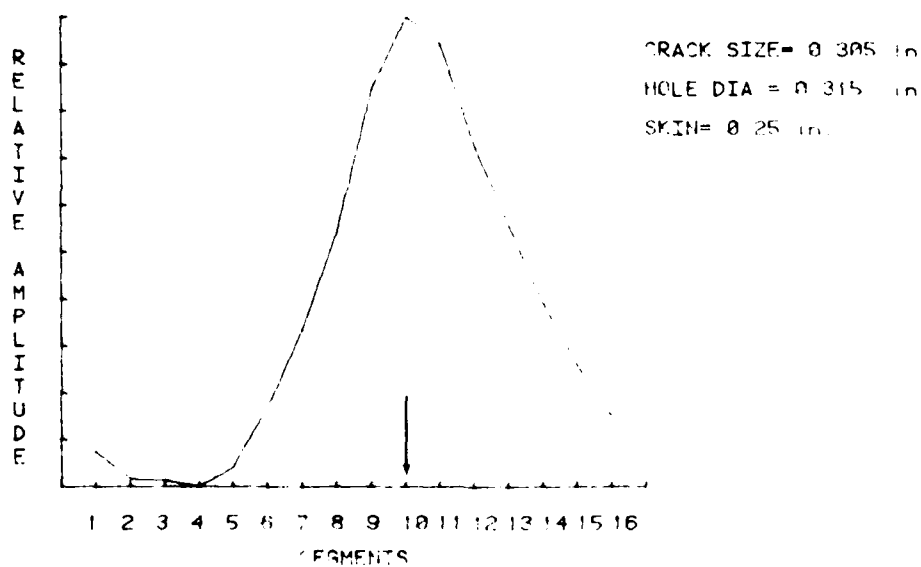


Figure 60. Detection Plot of GFM 'Specimen I', Hole 6

CRACK DETECTION UNDER INSTALLED FASTENER (Ti)

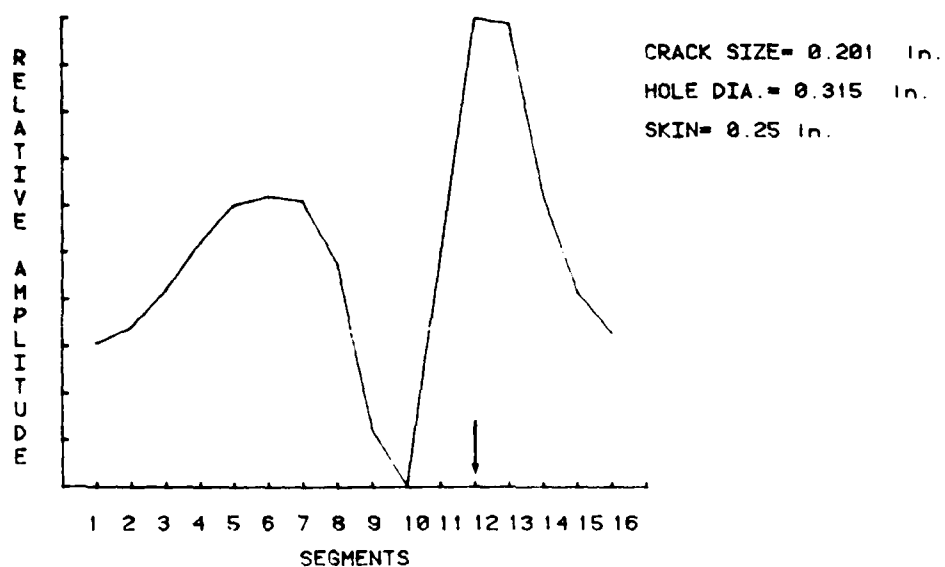


Figure 61. Detection Plot of GFM "Specimen I", Hole 15

CRACK DETECTION UNDER INSTALLED FASTENER (Ti)

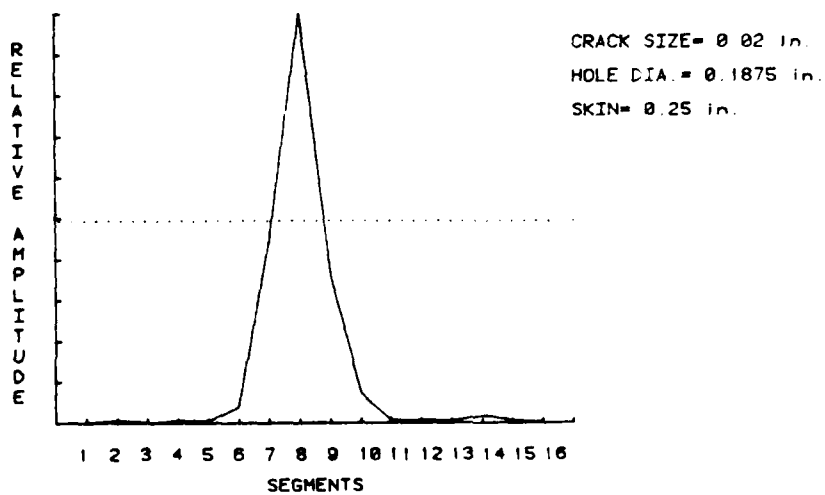


Figure 62. Detection Plot of an Outer Layer Flaw

SECTION 6

DISCUSSION OF RESULTS

Multisegment Probe

The multisegment array probe was the most promising one among the three. It was able to detect second layer flaws as small as 0.04 inch through 0.25-inch first layer for Type I specimens as shown in Figures 33 through 41. Maximum voltage change occurred when the flaw was under the segment face at the edge of the fastener. Minimum voltages were from those segments that were oriented at 90 degrees with respect to the flaw where the changes in eddy current were almost zero. A smaller voltage change at 180 degrees or 8 segments away from the flaw was due to the back wall eddy current.

The effect of frequency variation was examined. When the operating frequency was too low, the driving coil would be close to short circuit and was not able to deliver any power. When the frequency was too high, the fields could not penetrate due to the skin depth. Operation between 3000 Hz and 700 Hz was found satisfactory. Four hundred Hz was chosen because overall it seemed to give the best signal to noise ratio and the sharpest crack slope indication.

For Type II specimens or skin splice coupons, if the flaw is toward the splice, the relative position of the probe is not crucial. Rotation of the probe by one segment or 22.5 degrees caused only slight increase in background noise, but it still indicated crack orientation correctly. However, when the flaw is away from the splice, the splice or seam effect would mask the crack signal as shown in Figure 49. The crack was on segment 1, but it was indicated by segment 11.

Similar problems were experienced on Type III or structural edge coupons. When the flaw was toward the edge, small shifts of the probe had little effect on detection ability. But when the flaw was away from the edge and probe was shifted, it would interfere with the probe's ability to detect flaws. In Figure 53, the crack was on segment 1; however, it was indicated by segment 6.

For simulated material, the sealant condition seemed to have no effect on the performance of the probe.

Crack indication curves for GFM detection were slow varying compared to simulated specimens. The smoothing effect may be due to the combination of splice, edge and thickness variation of the GFM specimens.

Detection of outer layer flaws were equally as effective. There was no need for separate probes or processing electronics for inner and outer layer flaw detections.

Three-Phase Probe

The three-phase probe was unable to detect a 0.1 inch inner layer flaw if the outer layer was more than 0.080 inch thick. Several probe geometries were tried within reasonable limits of probe size and construction complexity. However, it still failed to detect second layer flaws of a 0.1 inch in radial length if the first layer was 0.25 inch or thicker. The reason for the detection difficulty for the three-phase probe is still not fully understood.

Quad Cup Probe

Preliminary tests on the quad cup probes revealed that the fields do not rotate around the fastener hole in the manner predicted by the analysis. In the absence of pole shaping the rotation fields were expected to be non-uniform. An attempt to make the fields more uniform by introducing more segments made the configurations impractical when compared to the multisegment probe. Consequently, the probe would require a mechanical rotation around the fastener in order to make a complete 360 degree inspection. A second layer crack in the order of 0.1 inch can just barely be detected through an 0.25 inch first layer only when the flaw falls under one of the legs of the quad cup probe. The reason for this failure is not fully understood at the present time.

SECTION 7

CONCLUSIONS

The program objective has been obtained and fully demonstrated. It was gratifying to discover the great sensitivity of the array probe to detect second layer notches as small as 0.04 inch through 0.25 inch in the first layer. However, angular probe positioning and boundary effects remain a problem.

The unique features of this array probe for application to second layer cracks in bolt holes are:

1. The probe reveals the local variations in eddy currents rather than the integrated result of the entire distribution; therefore, the flaw orientation can be determined.
2. The circumference of the hole is scanned electronically rather than mechanically. This feature significantly reduces errors due to liftoff and centering.
3. Electronic centering is achieved with the same probe.
4. Inspection of the holes is accomplished with the fasteners in-place.
5. The probe is not affected adversely by the sealant material used between the layers being held together by the fastener.

SECTION 8

RECOMMENDATION FOR FUTURE WORK

Although the basic feasibility of LFEC circular array probe for detection of cracks under installed fasteners has been demonstrated, further work is required to fully assess the technique. Some of the important areas worthy of further study are the following:

- Geometry Improvement - It must be recognized that the probe design was not optimized for any particular fastener configuration. More work should be done to optimize the probe geometry such as number of segments, center pole diameter, segment width, distance between center pole and outer segments, etc. Maximum performance can be obtained by varying the above parameters.
- Outer Layer Cracks - The work so far has concentrated on inner layer cracks, but there are strong indications that the array probe is more sensitive to outer layer cracks. The multifrequency capability of this probe for detection and measurement of first and second layer cracks should be evaluated.
- Field Application - Microprocessors and related hardware now make possible the development of a low-cost portable scanning unit for field use. By incorporating the techniques presented here and the data acquisition/analysis capability of the microprocessor, an inspector can use the instrument to locate cracks under installed fasteners and classify them in real-time, without operator interpretation or decision required.
- Boundary Effect and Self Calibration - There is a great need to study the effect of boundary conditions on the reliability of the crack detection. As discussed in Section 6, the reference piece and test specimens have to be identical and probe position is crucial. This is because, for the case of second-surface crack in bolt holes with fasteners in place, the flaw induced field changes are much smaller due to shielding by the first layer

and due to the distance between the crack and the segments. However, in the real world, a precise reference for every fastener hole is impossible. Therefore, it is necessary to do the segment calibration in-place rather than on a separate reference specimen and then transfer to the specimen of interest. This procedure would be required if the error voltage caused by inaccuracies in coil placement exceed the voltage change due to the flaw itself. However, by operating the coil at a higher frequency where the flawed region is cutoff due to skin effects, then any variations between segment voltages may be accounted for. If this standardless reference technique works, then the probe will be insensitive to any boundary or geometry effects. Also, the nature of error voltage versus segment position must be analyzed in greater detail in order to quantify the actual crack information such as size and orientation.

APPENDIX A

PHOTOGRAPHS OF GFM SPECIMENS

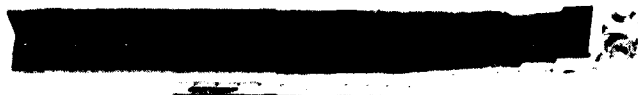


INNER LAYER SURFACE



OUTER LAYER SURFACE

Figure A-1. Photographs of GFM 'Specimen A'



INNER LAYER SURFACE



OUTER LAYER SURFACE

Figure A-2. Photographs of GFM "Specimen B"



NO. 1 100133

INNER LAYER SURFACE



NO. 1 100133

OUTER LAYER SURFACE

Figure A-3. Photographs of GFM "Specimen C"

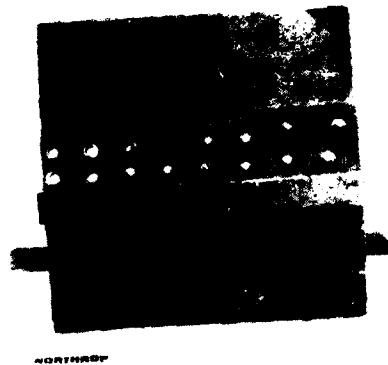


INNER LAYER SURFACE



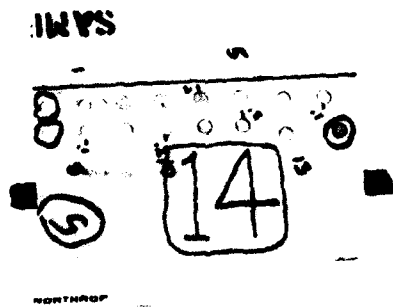
OUTER LAYER SURFACE

Figure A-4. Photographs of GFM "Specimen D"



NORTHROP

INNER LAYER SURFACE



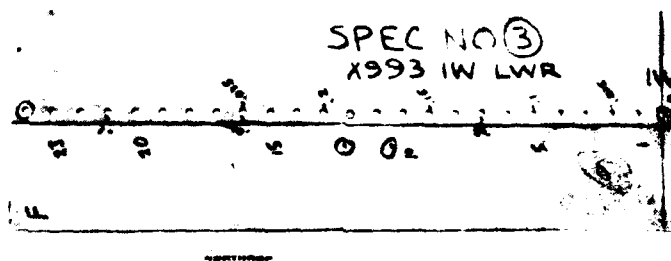
NORTHROP

OUTER LAYER SURFACE

Figure A-5. Photographs of GFM 'Specimen E'



INNER LAYER SURFACE



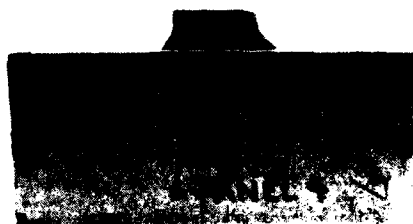
OUTER LAYER SURFACE

Figure A-6. Photographs of GFM "Specimen F"



NORTHROP

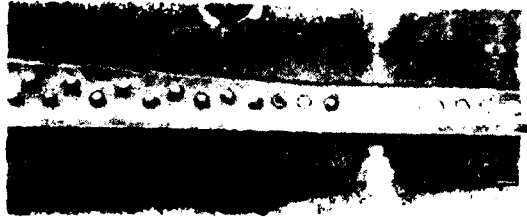
INNER LAYER SURFACE



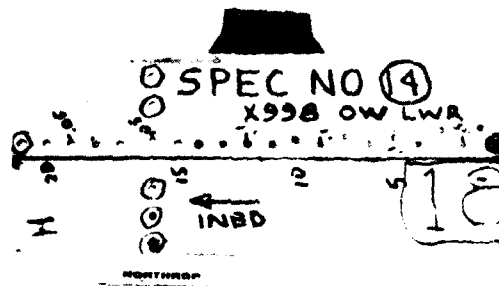
NORTHROP

OUTER LAYER SURFACE

Figure A-7. Photographs of GFM "Specimen G"

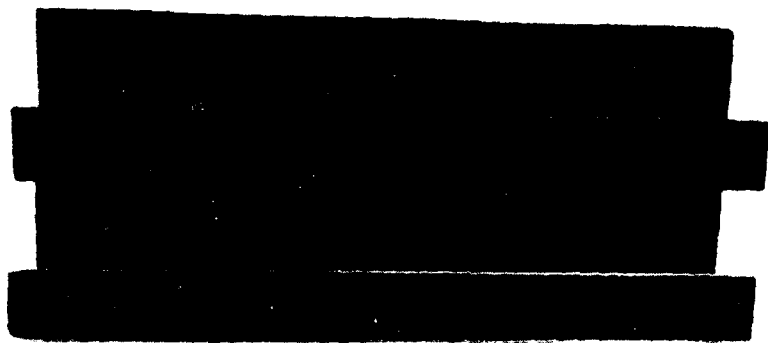


INNER LAYER SURFACE

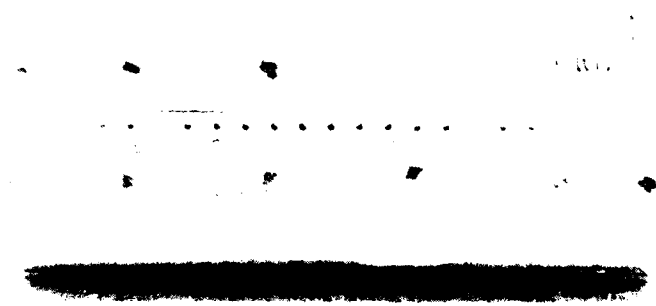


OUTER LAYER SURFACE

Figure A-8. Photographs of GFM 'Specimen H'



INNER LAYER SURFACE

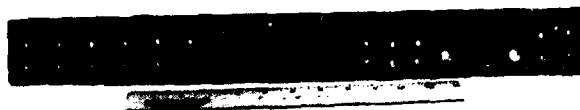


OUTER LAYER SURFACE

Figure A-9. Photographs of GFM "Specimen I"



INNER LAYER SURFACE



OUTER LAYER SURFACE

Figure A-10. Photographs of GFM "Specimen J"

APPENDIX B

GFM NOTCH DIMENSIONS

TABLE B-1. GFM "SPECIMEN A" NOTCH DIMENSIONS

SLOT LOCATION (hole number)	SLOT SIZE mm (inch)	SLOT ORIENTATION (in relation to splice)
2	3.81 (.15)	Away
6	1.91 (.075)	Away
11	1.91 (.075)	Away
14	2.54 (.1)	Away
20	2.54 (.1)	Away

NOTES:

1. Total number of fastener holes. 20
2. Number of holes slotted 5
3. Nominal Hole Diameter5/16 inch

TABLE B-2. GFM "SPECIMEN B" NOTCH DIMENSIONS

SLOT LOCATION (hole number)	SLOT SIZE mm (inch)	SLOT ORIENTATION (in relation to splice)
1	2.54 (.1)	Away
5	7.62 (.3)	Away
12	2.54 (.1)	Away
16	1.91 (.075)	Toward
19	2.54 (.1)	Toward

NOTES:

1. Total number of fastener holes 21
2. Number of holes slotted 5
3. Nominal Hole Diameter. 1/4 inch

TABLE B-3. GFM "SPECIMEN C" NOTCH DIMENSIONS

SLOT LOCATION (hole number)	SLOT SIZE mm (inch)	SLOT ORIENTATION (in relation to splice)
9	2.54 (.1)	Away
14	5.08 (.2)	Away
17	2.54 (.1)	Toward
19	5.08 (.2)	Toward
22	2.54 (.1)	Toward*
26	3.81 (.15)	Toward*
31	1.91 (.075)	Toward*
33	5.08 (.2)	Toward*

NOTES:

1. Total number of fastener holes 41
2. Number of holes slotted 8
3. Nominal Hole Diameter. 1/4 inch

* Relative to the closer splice.

TABLE B-4. GFM "SPECIMEN D" NOTCH DIMENSIONS

SLOT LOCATION (hole number)	SLOT SIZE mm (inch)	SLOT ORIENTATION (in relation to splice)
3	5.08 (.2)	Toward
5	2.54 (.1)	Toward
12	2.54 (.1)	Away
14	5.08 (.2)	Away
16	5.08 (.2)	Away
17	2.54 (.1)	Away
20	5.08 (.2)	Toward
23	2.54 (.1)	Toward
27	5.08 (.2)	Away
31	2.54 (.1)	Away

NOTES:

1. Total number of fastener holes 44
2. Number of holes slotted 10
3. Nominal Hole Diameter. 1/4 inch

TABLE B-5. GFM "SPECIMEN E" NOTCH DIMENSIONS

SLOT LOCATION (hole number)	SLOT SIZE mm (inch)	SLOT ORIENTATION (in relation to splice)
4	2.54 (.1)	Toward
7	2.54 (.1)	Away
8	2.54 (.1)	Away
10	5.33 (.21)	Away
12	5.08 (.2)	Toward

NOTES:

1. Total number of fastener holes 16
2. Number of holes slotted 5
3. Nominal Hole Diameter.5/16 inch

TABLE B-6. GFM "SPECIMEN F" NOTCH DIMENSIONS

SLOT LOCATION (hole number)	SLOT SIZE mm (inch)	SLOT ORIENTATION (in relation to splice)
2	1.91 (.075)	Away
5	2.54 (.1)	Away
7	5.08 (.2)	Toward
9	3.81 (.15)	Away
13	5.08 (.2)	Away
16	1.91 (.075)	Away
21	2.54 (.1)	Toward

NOTES:

1. Total number of fastener holes 25
2. Number of holes slotted 7
3. Nominal Hole Diameter.3/16 inch

TABLE B-7. GFM "SPECIMEN G" NOTCH DIMENSIONS

SLOT LOCATION (hole number)	SLOT SIZE mm (inch)	SLOT ORIENTATION (in relation to splice)
2	2.54 (.1)	Away
4	2.54 (.1)	Toward
8	5.08 (.2)	Away
11	5.08 (.2)	Toward
14	1.91 (.075)	Away

NOTES:

1. Total number of fastener holes 17
2. Number of holes slotted 5
3. Nominal Hole Diameter. 3/16 inch

TABLE B-8. GFM "SPECIMEN H" NOTCH DIMENSIONS

SLOT LOCATION (hole number)	SLOT SIZE mm (inch)	SLOT ORIENTATION (in relation to splice)
3	3.81 (.15)	Away
6	2.54 (.1)	Toward
9	2.54 (.1)	Away
12	2.54 (.1)	Away
16	1.27 (.05)	Away
19	1.27 (.05)	Away

NOTES:

1. Total number of fastener holes 26
2. Number of holes slotted 6
3. Nominal Hole Diameter. 3/16 inch

TABLE B-9. GFM "SPECIMEN I" NOTCH DIMENSIONS

SLOT LOCATION (hole number)	SLOT SIZE mm (inch)	SLOT ORIENTATION (in relation to splice)
2	5.08 (.2)	Away
4	1.91 (.075)	Away
6	7.62 (.3)	Toward
7	5.08 (.2)	Away
10	2.54 (.1)	Away
13	1.91 (.075)	Away
15	5.08 (.2)	Toward
17	3.81 (.15)	Away
19	2.54 (.1)	Toward

NOTES:

1. Total number of fastener holes 23
2. Number of holes slotted 9
3. Nominal Hole Diameter.5/16 inch

TABLE B-10. GFM "SPECIMEN J" NOTCH DIMENSIONS

SLOT LOCATION (hole number)	SLOT SIZE mm (inch)	SLOT ORIENTATION (in relation to splice)
3	5.08 (.2)	Away
5	2.54 (.1)	Away
7	2.54 (.1)	Away
10	5.08 (.2)	Away
11	2.54 (.1)	Away
13	2.54 (.1)	Away
16	3.81 (.15)	Away
19*	2.54 (.1)	Away
21	5.08 (.2)	Away
24*	5.08 (.2)	Away

NOTES:

1. Total number of fastener holes 30
2. Number of holes slotted 10
3. Nominal Hole Diameter.3/16 inch

* Hole Dia. 5/16"

